ADVANCING EARTH AND SPACE SCIENCE

Water Resources Research

RESEARCH ARTICLE
10.1029/2021WR030698

Toward a Closure of Catchment Mass Balance: Insight on the Missing Link From a Vegetated Lysimeter

Mitra Asadollahi[1], Magali F. Nehemy[2], Jeffrey J. McDonnell[2,3], Andrea Rinaldo[1,4], and Paolo Benettin[1]

[1]Laboratory of Ecohydrology ENAC/IIE/ECHO, École Polytechnique Fédérale de Lausanne (EPFL), Lausanne, Switzerland, [2]School of Environment and Sustainability, Global Institute for Water Security, University of Saskatchewan, Saskatoon, SK, Canada, [3]School of Geography, Earth & Environmental Sciences, University of Birmingham, Birmingham, UK, [4]Dipartimento ICEA, Università degli studi di Padova, Padua, Italy

Key Points:

- We combine data in a vegetated lysimeter with results from two transport models to contrast their convergence on an age-based mass balance
- We assess experimentally and computationally the interplay of advective and dispersive processes in driving the age of drainage waters
- We suggest the key control on the age selection by vegetation is root distribution, and propose a method to characterize its bulk effects

Supporting Information:

Supporting Information may be found in the online version of this article.

Correspondence to:

M. Asadollahi,
mitra.asadollahi@epfl.ch

Citation:

Asadollahi, M., Nehemy, M. F., McDonnell, J. J., Rinaldo, A., & Benettin, P. (2022). Toward a closure of catchment mass balance: Insight on the missing link from a vegetated lysimeter. *Water Resources Research*, *58*, e2021WR030698. https://doi.org/10.1029/2021WR030698

Received 26 JUN 2021
Accepted 21 MAR 2022

Abstract

Plant transpiration plays a significant role in the terrestrial cycles, but the spatiotemporal origins of water used by plant remains highly uncertain. Therefore, the missing link to fully characterize the water mass balance, for any control volume including significant vegetated surfaces, is identifying and quantifying the key factors that control the age of water used by plants. Here, we bring together an age-based (*tran*-SAS) and a physically based (HYDRUS-1D) model contrasting information gleaned from soil, drainage, and xylem samples at stand scale. In particular, we focus on the relative role of advection, dispersion, and root distribution on the age of water uptake and drainage. We suggest that the interplay of advective and dispersive forces, subsumed by the local Péclet number, drives the age composition of drainage even in the case of extreme uptake rates. The vegetation influence on the age of drainage is mainly exerted by diversifying the subsurface transport pathways resulting in large dispersivity and spatial heterogeneity of soil hydraulic parameters. We introduce a uniform-equivalent root length for vegetation and show that its ratio to the effective size of the subsurface water storage controls the age selection of water uptakes. Our results are suggestive of a route forward toward a general toolbox to upscale mass balance closures for catchments embedding large and diverse plant assemblages.

Plain Language Summary

Mass balance, the fundamental tool of hydrologic analysis, cannot be closed experimentally at the scale of a hydrologic catchment without answering a simple question: what waters do plants uptake? The characterization of vegetation abstractions, subsumed by water age in the transport volume, requires detailed knowledge of suitable chemical signatures of inflows and outflows and the fate of hydrologic waters by transport. In this study, we combine two conceptually different mathematical models with high-resolution experimental data (including tracer data from plants' xylem) to identify the main factors determining the origin of water used by vegetation. We suggest that a definition of a uniform-equivalent root length parameter proves significant in characterizing the age of plant uptake.

1. Introduction

Soil water-plant interaction accompanied by the uptake of nutrients is a key element in closing water and nutrient cycles at all spatiotemporal scales (Fatichi et al., 2016) with significant implications in ecohydrology, climatology, plant physiology, and biogeochemistry (e.g., Feldman et al., 2021; Grossiord, Gessler, Granier, Pollastrini, et al., 2014; Johnson & Jost, 2011; Porporato et al., 2004). However, the origins of water used by plants and their main controls are still poorly understood (e.g., Allen et al., 2019; Brooks et al., 2010; Dubbert et al., 2019; Dubbert & Werner, 2019; Sprenger & Allen, 2020; von Freyberg et al., 2020), especially when abstractions from large assemblages of plants are of interest (Rinaldo et al., 2015). In this context, both soil characteristics (e.g., soil hydraulic parameters) and plant features (like e.g., those of the rooting system) play a role in determining the origin of water used by plants, yet their relative role and mutual interactions in assessing the features of abstracted water remains uncertain to date. This gains traction in connection with the overarching problem of moving from the one-plant experimental framework to the much-needed understanding of the collective behavior of large and diverse assemblages of vegetation, the quintessential catchment scale. Current technologies do not allow us to do so. To that end, this work proposes to inch toward progress in the direction of experimentally closing the mass balance, for large multiplant hydrologic control volumes, by exploiting a cutting-edge experiment on a vegetated lysimeter (Benettin, Nehemy, Asadollahi, et al., 2021; Benettin, Nehemy, Cernusak, et al., 2021; Nehemy

et al., 2021) suggesting environmental controls possibly amenable to link remotely acquired and objectively manipulated information.

Considering the links between soil moisture dynamics and plant water uptake, how can we track the spatio-temporal origin of water taken up by plants? Transport models from plot to catchment scale based on different concepts account for water uptake dynamics with varied levels of complexity. These models can be classified as: (a) Models that explicitly account for the space heterogeneity and flow pathways known as space-explicit or physically based models (e.g., Feddes et al., 2001; Simunek et al., 1998, 1999; Sprenger, Tetzlaff, Buttle, Laudon, Leistert, et al., 2018); (b) Age-based or space-implicit models that use travel time distributions (TTD) concept, where TTD is proportional to the mass of an individual pulse of rainfall in the subsurface (water parcel) that has passed a point at time t, and TTD shape intend to reflect an integration of the undergone transport processes (e.g., Benettin & Bertuzzo, 2018; Harman et al., 2011; Van Der Velde et al., 2012); (c) Process-based models that incorporate age estimations (e.g., Kuppel et al., 2018; Maxwell et al., 2019; Remondi et al., 2018).

Tracer experiments enable tracking the fate of precipitation or irrigation events. They improve our understanding of the intertwined subsurface processes relevant to uptake processes. Therefore, conservative tracer measurements in combination with models have been used to make inferences on vegetation water uptake dynamics at lysimeter scale (e.g., Pütz et al., 2016; Quade et al., 2019; Queloz et al., 2015; Stumpp et al., 2009; Wenninger et al., 2010) or on evapotranspiration as a lumped parameter at site to catchment scale (e.g., Bertuzzo et al., 2013; Buzacott et al., 2020; Sprenger et al., 2016; Sprenger, Tetzlaff, Buttle, Laudon, & Soulsby, 2018; Van der Velde et al., 2010).

Within the domain of available conservative tracers to characterize the age dynamics, water stable isotopes of hydrogen and oxygen were proposed as the potential ideal tracer (e.g., Brunel et al., 1995; Ehleringer & Dawson, 1992; Kendall & McDonnell, 1998; Penna et al., 2018). When studying the age of water uptake by plants, not only the soil water mass exchange (lack of retardation and chemical reaction) matters, but also vegetation should sample the conservative tracer from the soil medium with similar affinity as water (e.g., Kendall & McDonnell, 1998; Mook & Rozanski, 2000; Zhang et al., 2010; Zimmermann et al., 1967). Concurrently, many works have suggested (or shown) that the reliance on stream or drainage data does not necessarily reflect vegetation water abstraction dynamics at the catchment scale (e.g., Benettin et al., 2017; Brooks et al., 2010; Evaristo et al., 2015; Goldsmith et al., 2012; McCutcheon et al., 2017; McDonnell, 2014). Moreover, even at a lysimeter scale with relatively low levels of uncertainty and well-known boundary conditions, the sole reliance on drainage characterization may result in different inferences on the age of water used by plants (e.g., Asadollahi et al., 2020). After earlier evidence showing distinct origins and ages between transpiration and streams (Brooks et al., 2010; Goldsmith et al., 2012), several studies collecting isotopic tracer directly from plants have appeared (e.g., Allen et al., 2019; Evaristo et al., 2019; Geris et al., 2017; Volkmann et al., 2016). As the method for quantification of plant water use at field or catchment scale remains a technological challenge and our current knowledge is limited in understanding water uptake dynamics in mixed cultured environments (but see e.g., Cabal et al., 2020; Volkmann et al., 2016), more research is needed (e.g., Brinkmann et al., 2018; Seeger & Weiler, 2021). In this framework, systematic studies to link physically measurable or remotely accessible information (say, plant model parameters such as root length density and parameters demanded by soil retention curves) are vital but missing, especially on the linkage of the water age in the transport volume (and thus its chemical composition, e.g., Li et al., 2021) and water uptake. Therefore, this paper attempts a first response to a call (Sprenger et al., 2019) to step away from modeling concepts that directly account for spatial heterogeneity, possibly to resort to age-based models that track ensembles of rainfall events.

Here, we combine two modeling approaches (age-based and physically based) with experimental data from a high-resolution controlled vegetated lysimeter experiment which has allowed empirical closure of mass balance for a single doubly labeled water injection (Benettin, Nehemy, Asadollahi, et al., 2021; Benettin, Nehemy, Cernusak, et al., 2021; Nehemy et al., 2021). We leverage this unique design with known boundary conditions and fine root distribution to understand if: (a) The observed gap between these space-explicit and space-implicit classes of model in the work by Asadollahi et al. (2020) persists in the presence of xylem data; (b) Combined use of space-explicit and space-implicit models leads to a deeper understanding of plant water uptake? Therefore, our objectives are: (a) To confront these models' at plot scale with high-resolution synergistic data which includes direct observations from two genetically identical trees. (b) Identifying the seemingly more important parameters in determining the age of plants' water uptake and closing the gap between space-explicit and space-implicit

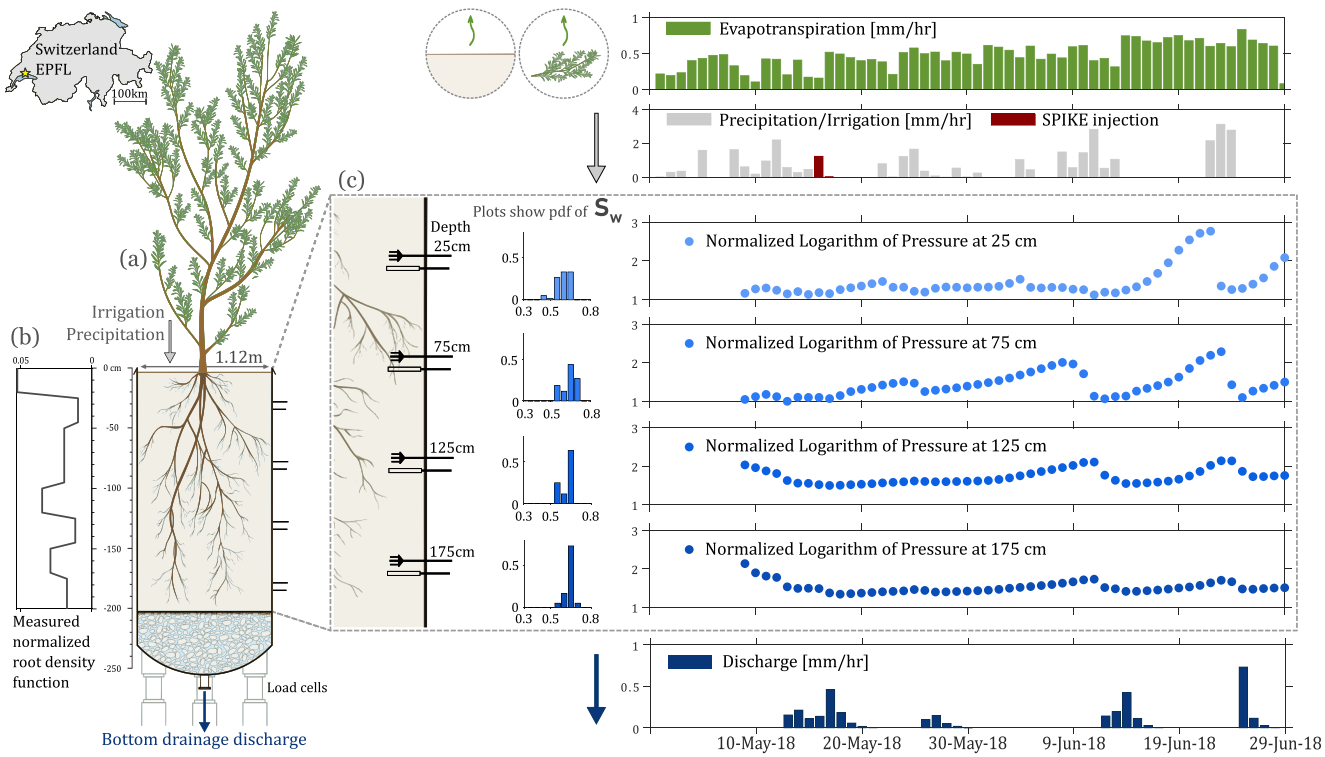

Figure 1. Illustration of (a) schematic sketch of the vegetated lysimeter located on École Polytechinque Fédérale de Lausanne (EPFL) campus, (b) directly measured normalized root length per volume of soil as a function of depth, (c) daily measured hydrological fluxes, temporal profile of normalized logarithm of pressure and histograms with soil moisture distributions at the different depths. The EPFL lysimeter with surface area of ~1.1 m^2 contained 2 m of soil and a 0.5-m gravel filter at the bottom. Two identical willow trees were inside the lysimeter and their roots were distributed along the entire soil column. The probability density function of saturation indicates variably saturated condition along the depth during the experiment. The pressure signal is generally responding faster to a precipitation event near the surface and the signal gets dissipated as it travels along the column. The SPIKE injection of doubly labeled water is marked with red color in the precipitation data.

model in this study; (c) Using this knowledge to find potentially a scalable method for catchment mass balance closure.

To achieve the above objectives, we first focus on utilizing a common Bayesian scheme for model calibration (Vrugt, 2016) and simulation of a SAS-based model, hereafter *tran*-SAS (Benettin & Bertuzzo, 2018) and a physically based model, hereafter HYDRUS-1D (Simunek et al., 1998; Stumpp et al., 2012). In the next step, we address the convergence between these two classes of models on the measured data which includes xylem isotopic composition measurements. Finally, we move to explore the role of different physical parameters on the age of transpiration and drainage via in silico experiments. In particular, we introduce a uniform-equivalent root length to show its key control on transpiration age dynamics under different flow regimes. We then discuss how this may serve as a first step in closing the water mass balance at catchment scales. To establish our finings, we strongly call for testing these finings under different sets of soil-plant-atmosphere continuum on several replicas.

2. Materials and Methods

2.1. Experimental Data: Mass Closure of a Tracer Injection

In this work, we used data from a water isotope tracer experiment (Benettin, Nehemy, Cernusak, et al., 2021; Benettin, Nehemy, Asadollahi, et al., 2021; Nehemy et al., 2021) that took place on EPFL campus in Lausanne, Switzerland, between May and June 2018, which was designed to trace one labeled injection in a hydrological control volume in the presence of two genetically identical willow trees (*Salix viminalis*), known for their relatively high transpiration rates (Lindroth & Cienciala, 1996).

As shown in Figure 1, data collection on lysimeter weight, pressure, and soil moisture started between May 1–5, 2018 (one measurement per 15 min). Soil moisture and pressure probes were located at depths 25, 75, 125 and

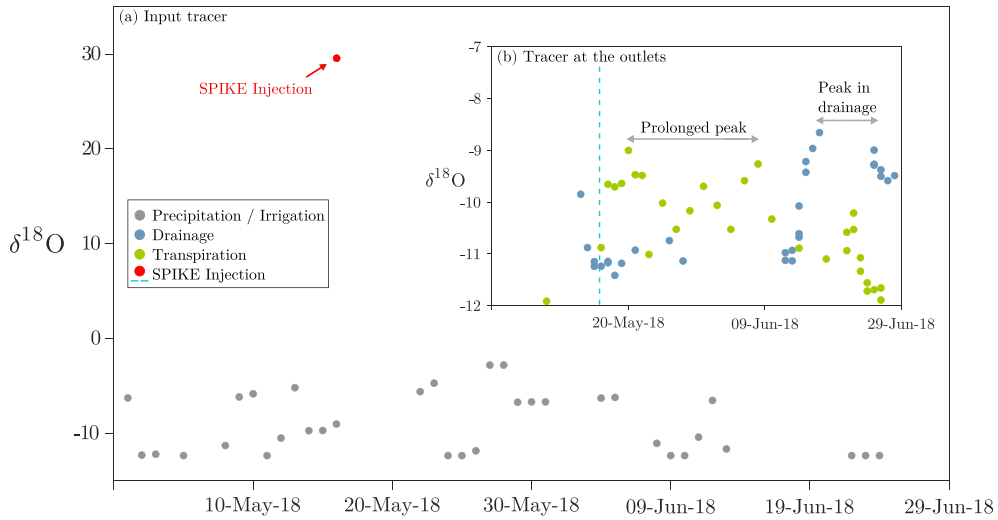

Figure 2. Demonstration of the measured tracer isotopic composition entering the soil column in precipitation and irrigation and exiting it in transpiration and drainage. In panel (a), the doubly labeled water injected at 23:00 on the May 16 is marked in red color. It stands out from the background isotopic tracer composition (gray dots). In panel (b), the measured tracer in both transpiration and drainage are shown at subdaily resolution. Samples are diluted after mixing with the water storage to a similar extent, and the timing for the peak at the bottom drainage flux approximately coincides with the falling peak in the transpiration flux.

175 cm (two probes at each depth). The lysimeter contained loamy sand and two willow trees with the height of approximately 2 m (the trees were planted in the lysimeter in 2012 and were regrown from a clear cut in 2014). This system was injected with 25 mm of a doubly labeled water tracer (hereafter also called SPIKE) over approximately 2 h, starting around 23:00 on May 16 The tracer was highly enriched in both δ^{18}O (+29.6‰) and δ^{2}H (+256.6‰). The lysimeter was subject to both precipitation and irrigation. The experiment ended on June 29 when we cut down the trees and characterized soil and trees isotopic composition, as well as trees' fine root density. It is also worth noting that transpired water was 99% composed of water uptake by trees' roots (Nehemy et al., 2021); therefore, we do not distinguish between age of root water uptake and transpiration in this work. In this context, we consider foliar uptake to be quantitatively negligible as the functional significance of foliar water uptake via fog or leaf wetting is relevant to certain species (Dawson & Goldsmith, 2018; Goldsmith et al., 2017), the amount of water contributing to transpiration via foliar water uptake is known to be small (e.g., Cavallaro et al., 2020; Limm & Dawson, 2010) and both location-dependent and species-dependent.

Tap water (used occasionally for irrigation), precipitation, and bottom drainage were sampled on an event-triggered basis. Bulk soil water samples were collected at 10, 25, 50, 80, 150 cm depths (two at each depth) on a 4-day basis (n = 120 in total). Xylem water was sampled at varied time intervals (maximum interval length of 4 days, and minimum of 6 hr: 56 in total). It is commonly assumed that transport of isotopes from root to xylem is a fractionation-free process (Dawson et al., 2002). Consequently, one can assume no isotope transformation occurred from root uptake to the xylem sampling point (and in particular, no fractionation). Figure 2 in panel (a) illustrates the SPIKE composition relative to the background precipitation and irrigation isotopic concentrations. The inset illustration in panel (b) of this figure shows the δ^{18}O isotope in xylem (source of transpiration) and bottom drainage water samples collected at subdaily frequency. Xylem and drainage isotopic concentrations were sampled prior to tracer application in order to estimate their background isotopic concentration. It is worth noting the similar magnitude in the peak of breakthrough curves at both outlets. The delayed decline in the prolonged peak in xylem samples' isotopic composition coincides with the emergence of a peak in drainage water isotopic composition. This is indicative of integration over similar spatial domain occurring at different times for both drainage and transpiration fluxes.

During the experiment, the weight of one adjacent soil-lysimeter (containing bare soil only) was monitored to estimate evaporation fluxes. As evaporation from bare soil is expected to be higher than the vegetated system, the ratio between the evaporation from the soil-lysimeter and the evapotranspiration from the willow-lysimeter together with the location of source samples on dual isotope plot indicated a partitioning of 10% for evaporation

and 90% for transpiration in the willow-lysimeter with an approximate uncertainty of 5%. Specific details on estimation of partitioning coefficient between evaporation and transpiration are included in a previous publication on this work (Benettin, Nehemy, Asadollahi, et al., 2021).

The enrichment of heavier isotopes in water due to evaporation (known as isotopic evaporative fractionation) affects ^{18}O and ^{2}H isotopes with different magnitudes and it makes them behave as nonconservative tracers. To avoid modeling the evaporative enrichment of the heavier isotopes, we compensated for the effect of fractionation "at the source", that is, directly in the isotope data. We used the approach by Bowen et al. (2018), which basically consists in assuming an evaporative enrichment trajectory and going backward along that trajectory until the enrichment is entirely removed. The approach takes into account various sources of uncertainty, including the slope of the evaporation line. The procedure is explained in more detail by Benettin, Nehemy, Asadollahi, et al. (2021). Therefore, measured isotope data used in this work and shown in this paper are fractionation-free. After removal of fractionation effects, the information content embedded in the two isotopes is the same and, to avoid redundancy, we only show results for $\delta^{18}O$.

All data used in this work are aggregated in space at the sampling point and averaged in time to *daily* resolution. For more details on the experimental design, measurement devices, sample storage, other data types collected during the experiment and their analysis, please, see works by Benettin, Nehemy, Cernusak, et al. (2021), Nehemy et al. (2021), and Benettin, Nehemy, Asadollahi, et al. (2021).

2.2. Transport Models: Calibration, Configuration, Simulation

We selected HYDRUS-1D modified for the transport of isotopes (Stumpp et al., 2012) as our spatially explicit model. In this version of HYDRUS-1D, evaporation has no effect on the remaining isotopic composition in the storage. Our spatially implicit model is *tran*-SAS (Benettin & Bertuzzo, 2018), which simulates flow and solute *tran*sport using "StorAge Selection" (SAS) functions. After initial testing to identify the appropriate spin-up period, the simulations started on May 1 (16 days prior to the labeled tracer application) to provide enough time for the models to reach equilibrium. The simulations ended on June 29 when the willow trees were cut down. Measured precipitation and its isotopic composition as well as evaporation and transpiration fluxes, separated by E/ET = 0.1 ratio (Benettin, Nehemy, Asadollahi, et al., 2021), are all inputs in both of these models. *tran*-SAS needed drainage as an additional input data while HYDRUS-1D simulates drainage but requires directly measured root density function as an input parameter. Based on bulk soil water samples collected in March and early May, in the models, we opted an initial isotopic composition of −12.64 [‰]. Both models were calibrated with global Markov Chain Monte Carlo (MCMC) optimization algorithm embedded in $DREAM_{zs}$ (Vrugt, 2016). It was assumed that the model residuals were normally distributed as this is a common assumption when the data are expected to have no bias. Different data types were used in these calibrations.

Following the recommendation of Groh et al. (2018) and Sprenger et al. (2015), the error for all individual data points is simultaneously utilized in the objective function to find the best parameter estimates. These computed errors are divided by the number of data points and the standard deviation in each data set to account for the varying magnitude among different sets. The calibration process stops when 2×10^4 runs in convergence is reached for all chains, more details on calibration and the method used to create a unified error vector are included in Supporting Information S1 (Section 1).

2.2.1. *Tran*-SAS Model

For $DREAM_{zs}$ calibration in *tran*-SAS, only the isotopic composition of the xylem and drainage were directly compared with *tran*-SAS outputs as, among the collected data types, none is directly extractable from *tran*-SAS (measured bottom drainage flux is a model input contrary to HYDRUS-1D where measured bottom drainage is a data set used for calibration). Therefore, simply the isotopic composition of the xylem and drainage data sets with a total of 46 data points (averaged to daily resolution) were used in the calibration process.

In this work, we modified the age master equation (Botter et al., 2011) in *tran*-SAS as illustrated in Equation 1 to separately account for the underlying age dynamics that drive evaporation and transpiration instead of using a lumped representation of the two in terms of evapotranspiration.

$$\frac{d}{dt}\left[S(t)p_s(T,t)\right] = J(t) - Q(t)\omega_Q(T,t)p_s(T,t)\ldots \\ -T(t)\omega_T(T,t)p_s(T,t) - E(t)\omega_E(T,t)p_s(T,t) \tag{1}$$

In this model, all rainfall and irrigation (combined into one term $J(t)$), bottom drainage $Q(t)$, evaporation $E(t)$, and transpiration $T(t)$ fluxes are a model input, and the resident time distribution in the storage, that is, $p_s(T, t)$ is solved in time. In this equation, SAS functions (ω) describe how each outflux selects from the pool of ages available in the storage. The age master equation in *tran*-SAS is expressed in cumulative form and the SAS functions are expressed in ranked storage, that is, $S_T(T,t) = S(t)\int_0^T p_s(\tau,t)d\tau$, to make the scheme more suitable for numerical implementation (Benettin & Bertuzzo, 2018; Harman, 2015).

During the first stage of soil evaporation, water is supplied to the evaporation plane at the soil surface via continuous liquid pathways driven by capillary gradients across a relatively shallow depth of 9–15 cm for coarse-to-fine-textured sand media, respectively (Lehmann et al., 2008; Or et al., 2013). In a vegetated soil surface, the shallow soil vaporization zone is further shortened given root water uptake exerting viscous losses that act against the capillary water supply to the surface (Haghighi & Kirchner, 2017). In a vertical soil column, one often expects a water parcel that has entered the system recently (younger storage) to be more abundant at shallower depths; and therefore, in age demographics of water a relatively young age leaves via the evaporation flux (Sprenger et al., 2019). Given these considerations, the SAS function for evaporation, that is, ω_E, is chosen to be a uniform-truncated step function where a cut-off parameter, that is, u_E, between zero and one limits the presence of older ages in ranked storage. For transpiration SAS function, that is, ω_T, a power function with coefficient k_T is selected to minimize the number of model parameters yet to allow for any age selection scenario. As shown in Asadollahi et al. (2020), drainage is typically produced by the oldest water components. For this reason, we used again a uniform-truncated SAS function for drainage but this time the uniform part samples the older water and not the younger water (hence, we call it inverse uniform-truncated).

The optimal SAS functions parameters, u_E, u_Q, and k_T, along with the initial lysimeter storage, S_0, were determined in the calibration process. Consistency of results has been tested by choosing varied shapes (beta function, piece-wise linear, etc.) of SAS function. It is worth to mention that, in drainage, the older water storage contribution to SAS function (ω_Q) was uncertain as hydrological data was available only for a duration of 60 days. Therefore, detailed explanation on best parameter when different functional forms are assumed for drainage SAS function are included in the Supporting Information S2 (Section 2 and Figure S1).

2.2.2. HYDRUS-1D Model

For DREAM$_{zs}$ calibration in HYDRUS-1D, we used bulk soil ($n = 12 \times 5$), xylem ($n = 26$), drainage ($n = 20$) water samples together with pressure ($n = 52 \times 4$), moisture ($n = 60 \times 4$), and drainage flow ($n = 60$) data (averaged to daily resolution): a total of 614 data points from six different data types.

We ran initial tests with different configurations (including dual porosity and separation between the soil column and the gravel filter), for more detail on separation between the soil column and the gravel filter see Supporting Information S3 (Section 3, Figures S2 and S3, Tables S1 and S2). We retained the uniform model configuration because it simulated the data equally well without additional complexity. In this configuration, the flow transport is based on Richards equation (Richards, 1931) in a vertical column as demonstrated in Equation 2:

$$\frac{\partial\theta}{\partial t} = \frac{\partial}{\partial z}\left[K(h)\left(\frac{\partial h}{\partial z}+1\right)\right] - (S_{w,T} + S_{w,E}) \tag{2}$$

where θ is volumetric water content [$L^3\,L^{-3}$], t is time [T], z is depth below surface (positive upward) [L], K is soil hydraulic conductivity [$L\,T^{-1}$], h is soil water pressure head [L], and $S_{w,T}$ and $S_{w,E}$ are sink terms due to root water uptake and evaporation from a unit volume of soil per unit time [T^{-1}]. The functional forms of soil water retention curve $\theta(h)$ and hydraulic conductivity $K(h)$ are based on the Mualem-van Genuchten approach (Mualem, 1976; Van Genuchten, 1980), where empirical parameters n [–], α [L^{-1}], saturated and residual water content, that is, θ_s and θ_r, and saturated hydraulic conductivity K_s define the shape of these functions.

Tracer transport in HYDRUS-1D uniform model is based on advection-dispersion as shown in Equation 3:

$$\frac{\partial(\theta C)}{\partial t} = \frac{\partial}{\partial z}\left(\theta D\frac{\partial C}{\partial z}\right) - \frac{\partial(qC)}{\partial z} - (S_{C,T} + S_{C,E}) \tag{3}$$

where C corresponds to δ^{18}O in soil water [$M\,L^{-3}$], D is hydrodynamic dispersion coefficient [$L^2\,T^{-1}$], and q is the water flux [$L\,T^{-1}$]. $S_{C,T}$ and $S_{C,E}$ are sink terms of tracer concentration due to root water uptake and evaporation from a unit volume of soil per unit time [$M\,L^{-3}\,T^{-1}$], respectively. In this version of HYDRUS-1D, the sink term for tracer concentration due to evaporation ($S_{C,E}$) is defined as $S_{w,E} \cdot C$ (the sink term for evaporation flux multiplied by soil concentration). Additionally, we defined the tracer concentration sink term due to transpiration ($S_{C,T}$) as $S_{w,T} \cdot C$ such that water extraction by plant will not have any impact on the remaining isotopic concentration in the storage. Measured and estimated atmospheric fluxes (precipitation, transpiration, and evaporation) at the top and seepage face ($h = 0$) at the bottom are the boundary conditions used in the simulations. Hence, the initial pressure distribution in the soil assumes an equilibrium condition and linear increase from the surface to reach a value of zero at the seepage boundary.

In this equation, the dispersion coefficient is expressed as $D = D_L \cdot v + D_w \cdot \tau_w$ where D_L is longitudinal dispersivity [L], v is the average pore water velocity [$L\,T^{-1}$] defined as q/θ, D_w is the molecular diffusion coefficient in free water [$L^2\,T^{-1}$], τ_w is the tortuosity factor in liquid phase [–] (Bear, 2012). As the transport of δ^{18}O isotope is modeled, dispersion coefficient can be simplified to $D = D_L \cdot v$.

To estimate the transpired water, that is, $S_{w,T}$ in the flow transport equation, a macroscopic model is used for root water uptake where the amount of transpiration is estimated independently from the flow equation. These models due to their effective simplicity and low computational cost are suitable for larger scale applications (Baram et al., 2016; Feddes et al., 2001) and serve our objectives in this study. Such models can be directly based on root to shoot pressure gradient (e.g., Couvreur et al., 2014) or indirectly account for plant regulation (e.g., Feddes, 1982; Jarvis, 1989; Šimůnek & Hopmans, 2009). Recent work by Cai et al. (2018) suggested that the parameters are transferable between the two models. Moreover, as our focus is on the age of water used by plants, gradient-based water uptake model is unnecessary.

To estimate root water uptake, the Feddes function is employed (Feddes, 1982). In this formulation, transpiration distribution along the soil relies on normalized root function (estimated from measured root length per volume of soil: RLD [$L\,L^{-3}$]) and is adjusted in quantity due to water availability, as illustrated in Equation 4:

$$S_{w,T}(z,t) = \alpha_{rw}(h(z))\, b(z)\, T_{meas}(t) \tag{4}$$

where measured transpiration rate at each time step, that is, $T_{meas}(t)$, is distributed along the soil column proportional to the normalized root length density function $b(z)$ [L^{-1}] defined as $RLD(z)/\int_0^{L_R} RLD(z)dz$ (with no effect on the total transpiration rate $\int_0^{L_R} b(z)dz = 1$) and then adjusted due to soil water availability. This adjustment is made when the *local* transpiration rate is multiplied by the corresponding *local* coefficient of stress response function obtained from the Feddes model, that is, α_{rw} ($h(z)$. This parameter is computed for every spatial grid in time and is expressed in terms of *local* soil water pressure head, $h(z)$. Transpiration is zero at extremely dry conditions (below wilting point, $h \le h_4$) and at conditions wetter than anaerobiosis point, that is, $h \ge h_1$. Under dry soil conditions ($h_4 < h < h_3$), the term h_3 and its dependence on plant's transpiration demand accounts for plant regulation. This means, as shown in Figure 3, when the soil is too dry ($h < h_3$) or too wet ($h > h_2$) at a certain depth, water uptake is estimated to be reduced and nonoptimal in that location. Thus, predicted modeled transpiration will be less compared to measured transpiration at that time. It is worth noting that when a compensated water uptake scenario is considered in Feddes model, modeled and measured transpiration will always remain equal in time as reduced uptake at one location is compensated by increased uptake at another location. For this reason in our configuration, transpiration rates estimated by model can be smaller than measured transpiration rates. The ratio of modeled transpiration rates over its measured quantities indicates the need for water uptake compensation if plant has been stressed due to lack of water availability in soil. In this experiment, this ratio is above 0.90 for all days with the exception of the following five dates: May 12 and June 11 and 23–25; suggesting a compensated root water uptake model is redundant (on these dates both soil is dry and trees experience water deficit as shown by Nehemy et al. (2021)).

Initially, we had different calibration runs with different subsets of HYDRUS-1D model parameters to identify the most important parameters and keep the number of parameters to the least. In the early calibrations, all or subsets of the Feddes model parameters (h_{3h}, T_{3h}, h_{3l}, T_{3l}, h_4, h_2) were included. The posterior distribution for all these parameters was uniform. Hence, only h_{3h} is kept in the final calibration for demonstration purposes. The possibility of compensated water uptake model where reduced water uptake at certain locations results in increased and compensated water uptake at other locations along the soil profile was considered in the early calibration, but

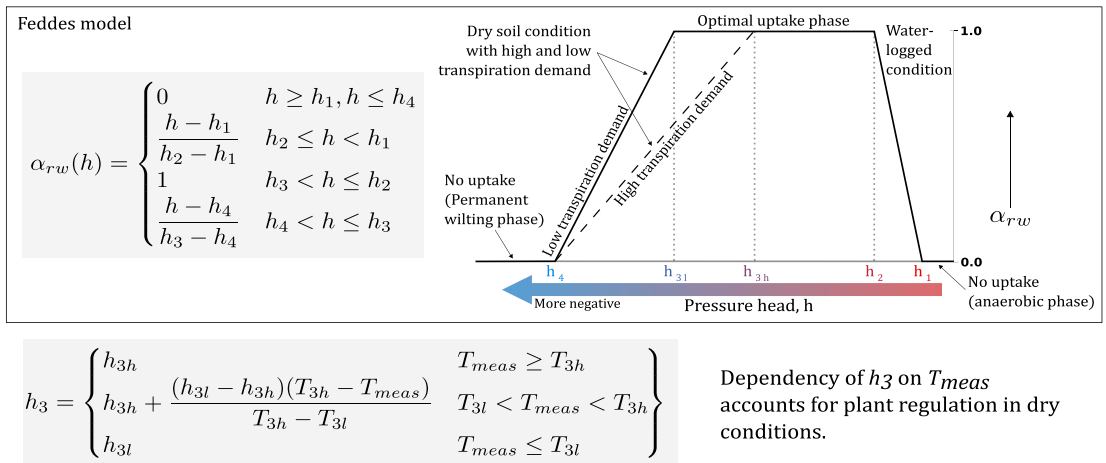

Figure 3. Illustration of the root water uptake stress response function α_{rw} without compensation in the Feddes model at the top and its dependency under drier soil conditions on plant transpiration demand at the bottom. In this model, tree response to waterlogged ($h_2 < h < h_1$) and dry soil conditions ($h_4 < h < h_3$) is expressed by terms of nonoptimal plant uptake. In addition, plant do not extract any water beyond its permanent wilting point h_4 and anaerobiosis point h_1.

the data favored a no compensation root water uptake scenario. In the final configuration, α, n, K_s are optimized from soil water retention parameters, D_L from advection-dispersion equation, and h_{3h} in the Feddes function are optimized. The rest of model parameters in Equations 2–4 were either estimated from measurements, best parameters in early calibrations, or set to mean values found in literature and HYDRUS-1D library. Supporting Information S4 (Section 4, Figures S4 and S5) illustrate measurement versus simulated data from HYDRUS-1D.

2.3. Age Statistics and SAS Computations

In this case study, the same procedure as stated in Asadollahi et al. (2020) is followed to compute SAS functions and age statistics from HYDRUS-1D. However, the duration of experiment (~60 days) in comparison with the maximum resident time in the storage was shorter; and therefore, the age distributions were truncated, that is, total recovered mass of virtual tracer is less than its injected mass. To improve our age estimations under this condition where total mass recovery is less than unity, the recovery factor at each k outlet, that is, θ_{Ok}, is estimated by normalizing the sum of recovered mass at all outlets to unity, that is, $\sum_{k=1}^{n} \theta_{Ok} = 1$. Also, to estimate the contribution of older water in HYDRUS-1D, an additional virtual tracer simulation is carried out to track the initial water storage, that is, old water.

In *tran*-SAS, the age statistics only depend on calibrated SAS functions and the time series of input and output fluxes.

3. Results

3.1. Model Calibration

The parameters' posterior distribution for HYDRUS-1D and *tran*-SAS is illustrated in Figure 4 selected from the last one thousand model parameters in DREAM$_{zs}$ after approximately 2×10^4 converged runs. Maximum aposteriori parameters (MAP) are indicated by the dots. The best parameters for HYDRUS-1D are 300 [cm d^{-1}] for saturated hydraulic conductivity (K_s), 0.06 [cm^{-1}] for α, 1.31 for n which are empirical parameters in the soil water retention curve, 72.25 [cm] for longitudinal dispersivity (D_L), and −8364.83 [cm] for h_{3l} in the Feddes function. The rest of model parameters were set to fixed values (not set to be calibrated). For the Feddes model, these fixed value parameters were as follows: h_1 −10 [cm], h_2 −25 [cm], h_{3h} −5,000 [cm], h_4 −15,000 [cm], T_{3h} 0.5 [cm d^{-1}], and T_{3l} 0.1 [cm d^{-1}]. Residual water contents (θ_r) were set to 0 [cm^3 cm^{-3}], and saturated water content (θ_s) was equal to 0.3 [cm^3 cm^{-3}]. The relatively high longitudinal dispersivity (D_L) may suggest spatial heterogeneity of flow paths distribution and hydraulic conductivity (Sudicky, 1986). We observed this high heterogeneity when we employed single-objective functions (calibration carried out based on a single data

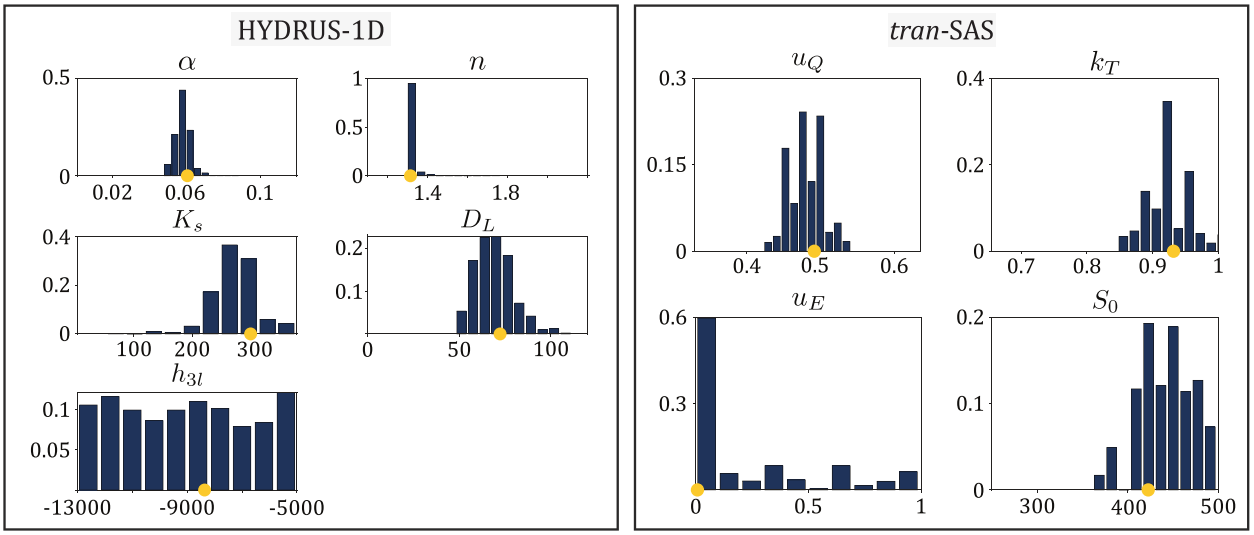

Figure 4. Posterior distributions of model parameters for HYDRUS-1D on the left and *tran*-SAS on the right is constructed based the last one thousand runs in DREAM$_{zs}$ after approximately 2×10^4 runs in convergence. The dots indicate the maximum aposteriori parameters (MAP) parameter.

set) in the calibration process and obtained highly varying estimates for saturated hydraulic conductivity K_s and slight variations in parameter α.

The MAP coefficient for the inverse uniform-truncated step function at drainage u_Q is 0.49 which may indicate that younger ages in the storage has exited the system due to evapotranspiration. For transpiration, optimal power coefficient, that is, k_T, is 0.93 which is very close to a random sampling. Finally, the MAP coefficient of uniform-truncated evaporation SAS function parameter u_E is 0.01 indicating the affinity for *very* young ages available in the storage. The best parameter for the initial lysimeter storage volume (S_0) is estimated to be 422 [mm] which is comparable with 362 [mm] obtained from HYDRUS-1D. In the HYDRUS-1D, the simulation with optimal model parameters yielded a maximum mass balance error of 1.1% for water transport and 0.5% for tracer transport.

3.2. Tracer Data Simulation

Figures 5a and 5b show the isotopic tracer breakthrough curve in drainage and xylem (source of transpiration), in sequence. The simulation uncertainty band is obtained by representing the 10–90 percentile, hereafter the 10–90 percentle, of one thousand simulation sets (input model parameters are drawn from parameter sets of posterior distributions in Figure 4). The measured data and its uncertainty have been aggregated to daily resolution (similar to simulation). The gaps in δ^{18}O breakthrough curve indicate the dates with no drainage flow. Both models generally match the tracer data in the transpiration and bottom drainage fluxes. In HYDRUS-1D, the isotopic concentration is slightly overestimated compared to the measured data and the *tran*-SAS prediction. This resulted in lower amount of δ^{18}O available in the storage; and therefore, a slight underestimation in the tracer peak at the bottom drainage.

A comparison is made between the modeled and measured normalized cumulative breakthrough curves (NCBTCs) in each outlet for SPIKE irrigation (Figure 6). For models, the normalized cumulative tracer mass recovery in each outlet is the product of cumulative forward travel time distributions multiplied by its corresponding ultimate recovery. In theory, these curves should be comparable with empirically obtained cumulative breakthrough curves normalized by the injected mass and corrected for background concentration in time as described by Benettin, Nehemy, Asadollahi, et al. (2021). The empirical NCBTCs and their associated standard deviations are shown in dotted lines in Figure 6. Modeled NCBTCs and the corresponding uncertainty band are shown by solid lines and colored bands, respectively. As mentioned before, the depth of soil evaporation is limited to shallow depths and as the labeled irrigation is transported downward along the column it becomes less likely to end up in evaporation. Therefore, the fraction of labeled irrigation's mass recovery in evaporation, see panel (a), reaches a plateau in a few days after the tracer application. Largest fraction of labeled irrigation is recovered

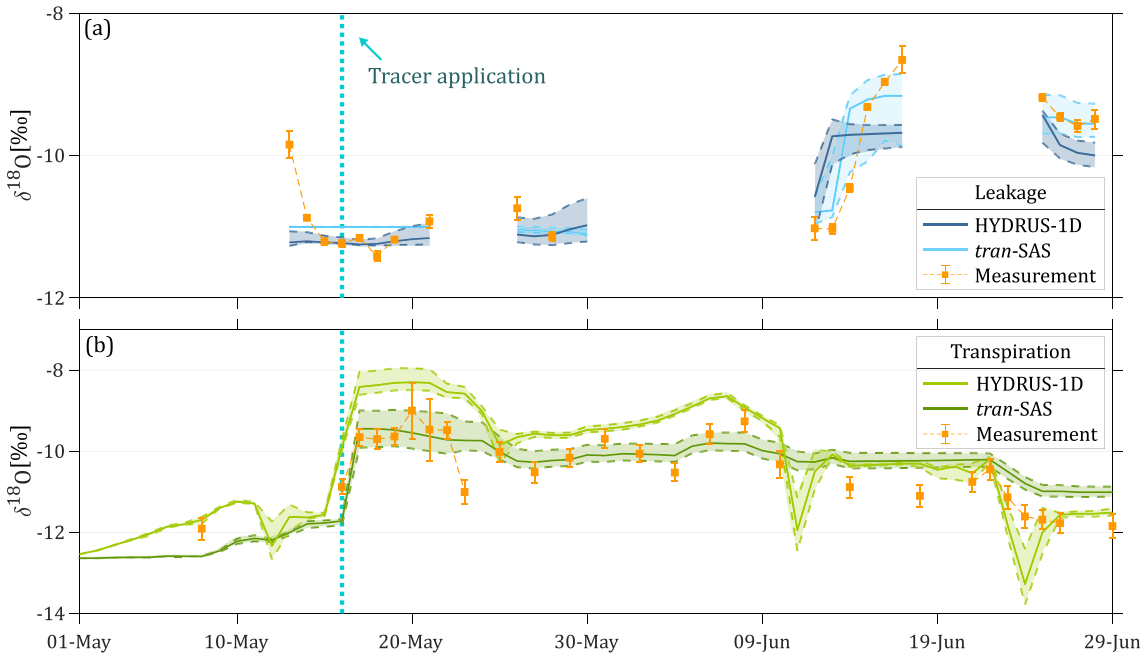

Figure 5. Illustration of measured breakthrough curve at transpiration and bottom drainage versus the modeling results in time. Panel (a) shows the model predictions for isotopic breakthrough curve in the drainage. Panel (b) illustrates δ^{18}O breakthrough curve in the transpiration. The solid lines and the band around them show the best parameter model simulation and the 10–90‰ of one thousand simulations with the parameters shown in posterior distribution (hereafter the 10–90‰), in order. Simulations are discontinuous when bottom drainage is zero; and thus, no sample could have been collected at drainage. The vertical dashed line shows the time for tracer application in both plots.

in transpiration as shown on panel (b). While *tran*-SAS outperforms HYDRUS-1D in predicting the measured NBTC in the first 20 days, HYDRUS-1D simulates better the mass recovery in transpiration from day 20 to the end of experiment. A clear explanation for this observation is missing. For the drainage shown on panel (c), despite the similar dynamics, we observe a difference of 5% in the estimated final recovery between empirical and modeled predictions while both models provided similar projections. The reason for this observation can be traced to the mismatch between the background concentration predicted by the models and the empirically estimated background concentration for drainage.

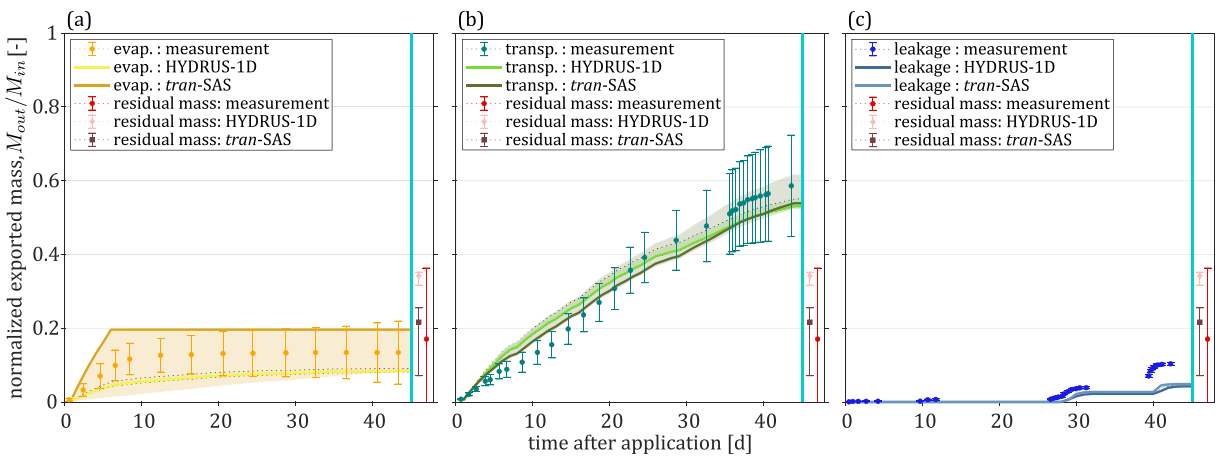

Figure 6. Modeled and measured normalized cumulative breakthrough curves (NCBTCs) of injected SPIKE that are normalized by the input mass and corrected for background concentration. The dots with error bars refer to NCBTCs derived from measured data and their standard deviation. The solid line and the highlighted area indicate the best model performance and the uncertainty band.

Table 1
Ultimate Recoveries Estimated From Measured Data and Models and Expressed in Percent

	BE	Min	Max		BE	Min	Max		BE	Min	Max
E_m	13	5	21	E_H	10	9	11	E_t	20	6	20
T_m	59	44	72	T_H	68	64	67	T_t	53	51	62
Q_m	10	10	10	Q_H	5	4	6	Q_t	5	3	6
Res_m	18	0	36	Res_H	17	17	20	Res_t	22	19	30

Note. The subscript *m*, *H* and *t* stand for measurement, HYDRUS-1D, and *tran*-SAS, in respect. BE refers to the best estimate while E, T, and Q refer to evaporation, transpiration, and drainage. For model predictions, min and max correspond to the minimum and maximum in the 10–90‰ of 1,000 simulations with parameters in the posterior distributions.

The modeled best estimate (BE) as well as the maximum and minimum predictions in the 10–90‰ for ultimate tracer mass recoveries in evaporation (E), transpiration (Tr), drainage (Q), and storage (residual mass: Res.) are summarized in Table 1. In this table, best estimates from empirical predictions are reported along with the minimum and maximum predictions (standard deviation of the best estimate). These values are expressed in percent and rounded for easier readability. It is worth to emphasize that while the numbers for best estimate add up to 100% (belong to one simulation), it is not the case for minimum and maximum values which mark the upper and lower bound of different simulations. These numbers are comparable with the ultimate recoveries shown in Figure 6.

3.3. Water Age Simulations

In Figure 7, the SAS function (shown on the *y* axis) based on calibrated parameters from *tran*-SAS are compared to the SAS function derived from HYDRUS-1D by daily virtual tracer simulations. The uncertainty band in *tran*-SAS indicates the 10–90‰ of SAS functions obtained from calibrated coefficients. In HYDRUS-1D, SAS functions were computed by tracking virtual tracer in the model that used the one thousand parameter sets shown in Figure 4. The 10–90‰ of these computed SAS functions are shown as uncertainty band in Figure 7. As computing SAS function in HYDRUS-1D involves tracking virtual tracer, it appears as a discrete function on dates where such tracking is not viable (e.g., days with no precipitation). In Figure 7, the *x* axis represents the normalized ranked storage, that is, $P_s = S_T/S(t)$. $P_s(T, t)$ is the volume of event waters available in the storage at time *t* that have entered the storage within the time lapse of zero to T. P_s of 1 indicates all previously precipitated water that is currently available in the storage while the value of 0.2 for P_s represents the 20% youngest water retained within storage. Both models show similar age selection at all storage exits. The drainage SAS function, in panel (a), is indicating extraction of older water in drainage by a nearly zero value at P_s below 0.2 (younger storage) and a relatively high value toward the end (older storage). The partitioning of evapotranspiration to transpiration and

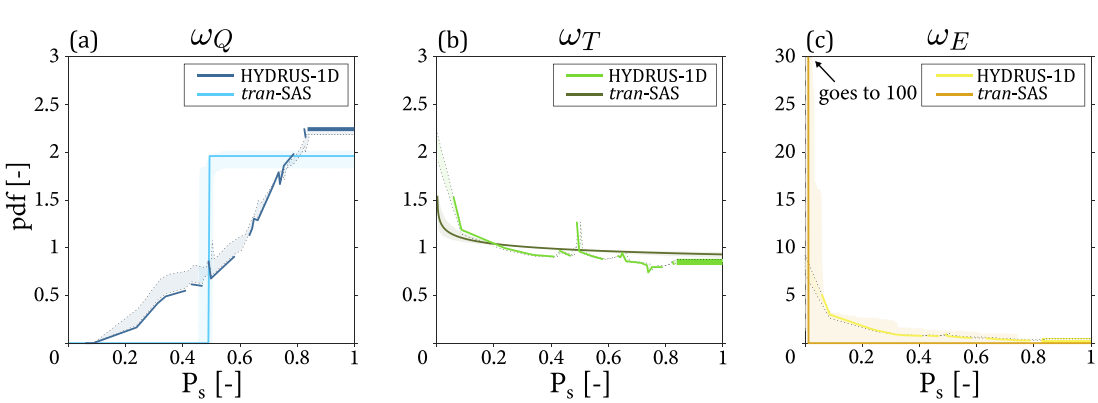

Figure 7. StorAge Selection (SAS) function at all exits: HYDRUS-1D versus *tran*-SAS. The solid lines show the SAS function corresponding to the best model performance. The uncertainty band refers to the 10–90‰ of one thousand obtained SAS functions. The *x* axis shows all ages of water retained within storage, and the *y* axis shows how an outlet is sampling from this pool of different ages. On panel (a), the SAS function in drainage (ω_Q) is shown (preference for older water available in the storage). In panel (b), the SAS function for transpiration flux (ω_T) is randomly sampling from the pool of ages in the storage. On panel (c), the SAS function for evaporation flux (ω_E) is shown (high affinity for youngest ages in the storage).

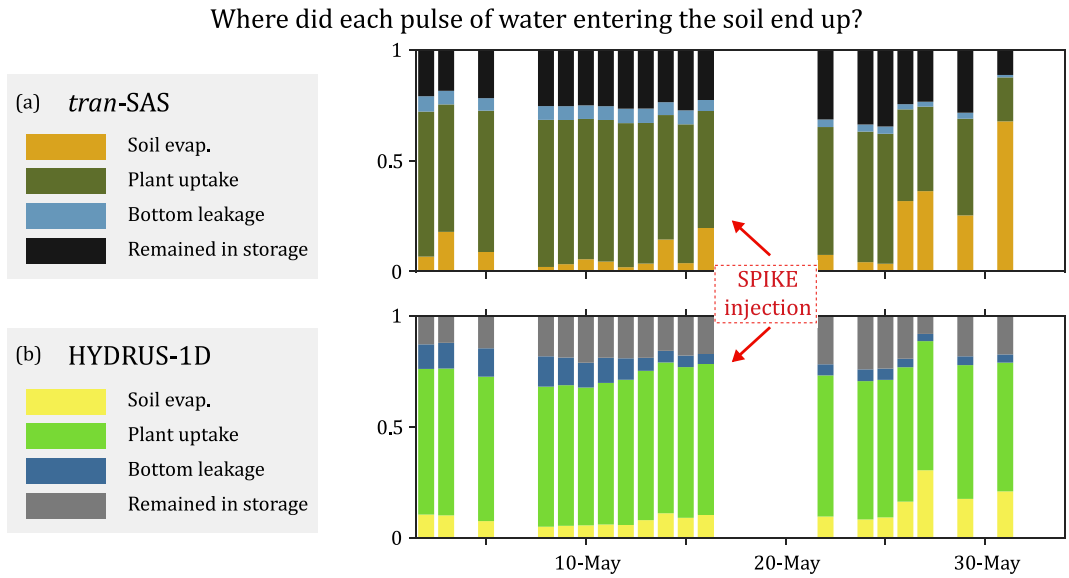

Figure 8. Predicted partitioning of event water among soil evaporation, vegetation abstraction, bottom drainage, and storage (mass remaining in the storage). Only predictions for events with less than 20% mass remained in the storage were considered as asymptotic estimates of the final partitioning coefficients when the event water remained the storage is zero or minimal. These asymptotic estimates can be compared across models.

evaporation flux results in quite different age dynamic for each, shown in panels (b) and (c). Evaporation fluxes represented preference for younger ages (the value of SAS function reaches a nearly zero value at P_s above 0.2) while transpiration is showing random sampling from all ages available in the storage (equal affinity for older and younger ages in the storage shown by the same value of SAS function for all values of ranked storage). As a result, contrasting the evaporation tracer dynamics against the tracer breakthrough curve measured at shallow depths in soil (not included in the calibration process) has been used to validate the models in Supporting Information S5 (Section 5 and Figure S6). In this experiment, accounting for interception would have a minor role on the age computations because interception evaporation was a very minor waterflux (more than 65% of the water input was provided as irrigation, thus bypassing the canopy entirely).

Figure 8 suggests that model predictions converge significantly on how much of an irrigation or precipitation event ended up in drainage, transpiration, evaporation or remained in the storage once the experiment ended. These predictions are expressed in terms of partitioning coefficients. For these partitioning coefficients at evaporation, transpiration and drainage to be a reliable approximation of the final partitioning coefficients, only the events that reached a total recovery of about 80% by the end of experiment are included. By final partitioning coefficients, here we mean the partitioning coefficients that would have been obtained if all the tracer mass had left the water storage (i.e., a total recovery of 100%). All precipitation and irrigation events in May 2018 met this criterion. The SPIKE injection is indicated with red arrows and its partitioning coefficients are equivalent to the ultimate recoveries demonstrated in Figure 6. For the injected SPIKE, in HYDRUS-1D, mean age of evaporation, transpiration and drainage were 8–10, 16–17, and 33–35 days, in sequence. In *tran*-SAS estimated mean age were 4–21, 18–20, and 35–37 days for evaporation, transpiration, and drainage, in order. These mean age estimates are comparable to the medians in Figure 6.

4. Discussion

Asadollahi et al. (2020) showed in a previous work that, even in the simple case of two monoculture lysimeter studies, sole reliance on bottom drainage flow and tracer data fails to result in similar predictions on the age of transpiration across HYDRUS-1D and *tran*-SAS models. Here, we explore the significance of simultaneous data collection from soil (tracer, water content, pressure) and plant (xylem tracer, and root length density) in bridging this observed gap between the two modeling approaches. After demonstrating the significance of this design in closing the mass balance at the stand scale, we aim to deconvolute the role of advective and dispersive forces

versus the plant root distribution on the age of drainage and transpiration through a series of virtual experiments via computing the SAS functions which intend to reflect the interplay between advection, dispersion, and root distribution elements.

4.1. Can Synergistic Collection of Tracer Data Bridge the Gap Between Modeling Approaches?

In Figure 7, we suggest equal affinity for uptaking younger and older ages of water available in the storage (also known as random sampling) by the *S. viminalis* trees in our experiment. It is remarkable that the random sampling scheme is consistently pointed at by the two models and the experimental observations. This finding is in contrast with the inference of plants using younger ages of water available in the storage made in a previous study (model combined with data) by Queloz et al. (2015) on the same lysimeter which contained the *very* same *S. viminalis* trees. Evolving root distributions may at least partially explain the coexistence of these two seemingly contrasting assumptions made on the age of water uptake from the same plant species in the same hydrological domain. This leads us further hypothesizing that the age of water used by plants is primarily driven by the root distribution. This is a reasonable hypothesis because the willows were originally planted by Queloz et al. (2015) in 2012 at the lysimeter top soil (0–50 cm depth). The trees were well-watered and grew for 2 years. Then, the willows were cut down in 2014 and regrown to be the subject of this experiment in 2018.

In Figure 8, the two models show similar predictions of how each event water was partitioned among different reservoirs. However, on May 27 and 31, when the amount of input water is less than 0.7 [cm d^{-1}] (about 50% of the averaged daily precipitation during the experiment, see Figure 1) and the storage volume is lower than its initial value ($\Delta S < 0$), the uncertainty in input-water partitioning to evaporation is rather high. For these precipitation events (May 27 and 31), HYDRUS-1D predicts more consistent, yet larger, partitioning coefficient for evaporation fluxes compared to the rest of the events considered. On the other hand, *tran*-SAS estimates most of the precipitated volume ending up in evaporation. This model prediction discrepancy can be traced to the fact that soil hydraulic parameters in HYDRUS-1D are calibrated against water retention data; such calibrations are shown to improve prediction of soil evaporation (Lehmann et al., 2020; Schneider et al., 2021) which has manifested itself under drier conditions in this study. The high uptake of water by trees is not exclusive to the labeled irrigation and applied to all rainfall or irrigation events with slight variations due to changes in environmental conditions including atmospheric forcing. Each rainfall event undergoes similar partitioning. The exceptions to this observation are days with low precipitation where water is limited and a higher fraction of event water returns to the atmosphere through evaporation. It seems what has remained from the event water after evapotranspiration goes to drainage. It is worth noting that these partitioning dynamics can be vary under different environmental conditions (e.g., in winter).

The results shown in this paper suggest that in the presence of extended experimental data (pressure, water content and tracer in soil, xylem, and drainage) models based on rather different premises provide a consistent interpretation of ongoing processes in terms of tracer simulation, age statistics, and storage sampling predictions for both drainage and transpiration, contrary to what has been observed elsewhere (Asadollahi et al., 2020).

To quantify the significance of xylem tracer data on the above convergence, we sought to calibrate both models in the absence of xylem tracer data. In absence of xylem tracer, the optimal parameters of the *tran*-SAS model are 0.6 for u_Q (similar to the previous results), while the optimal SAS function coefficients for evaporation (u_E) and transpiration (k_T) are equal, respectively, to 0.8 and 0.6 and initial storage is 252 [mm] (170 [mm] lower than *tran*-SAS calibration with xylem data). These coefficients misrepresent similar age dynamics for evaporation and transpiration, and lead to inappropriate inference on the age of transpiration (in particular with reference to the affinity for young water storage). In HYDRUS-1D, the best parameters are similar to previous estimates, 323 [cm d^{-1}] for K_s, and 52 [cm] for D_L. These parameters fall within the range of posterior distributions presented in Figure 4, and are close to the previously estimated optimal parameters. The performance of the models in terms of tracer breakthrough curves for transpiration and drainage obtained in this case, have been compared with the previous best models' performances (Figure 9). In all cases, tracer data in drainage are well predicted. However, in the absence of xylem data models no longer maintain similar predictions for the isotopic composition of the root uptake. We argue that this stems from model design. Indeed, physically based models can use all other sources of data (root length density, pressure, water content as well as soil tracer data) in addition to drainage tracer data, and their performance is relatively unaffected by the lack of information on transpiration isotopic composition (C_{Tr}). Moreover, the isotopic data of xylem water were already used to separate ET into E and T, and these data

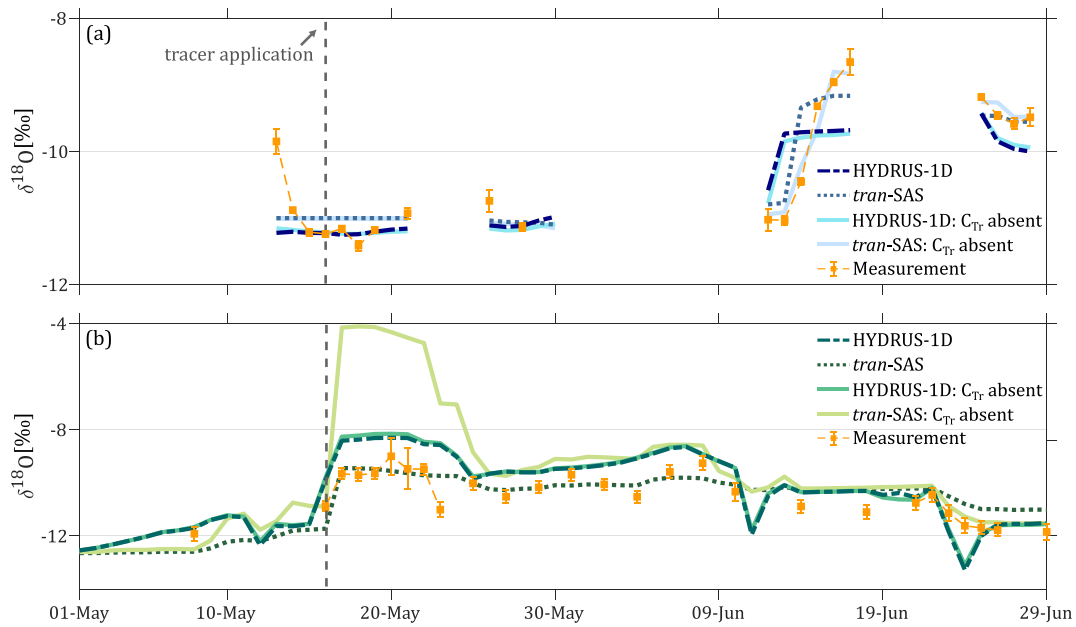

Figure 9. Comparison of optimal models' prediction on isotopic breakthrough curve in drainage, panel (a) and transpiration, panel (b), under two scenarios: (a) When source of transpiration (xylem) isotopic composition is absent; (b) When xylem isotopic composition is present. The sole reliance on drainage flow and tracer data (in SAS-based model) results in wrong predictions on isotopic breakthrough curve in transpiration. HYDRUS-1D as a physically based model is not affected by the absent of xylem isotopic composition as it already accounts for root length density function and additionally benefit from pressure, water content, and soil data.

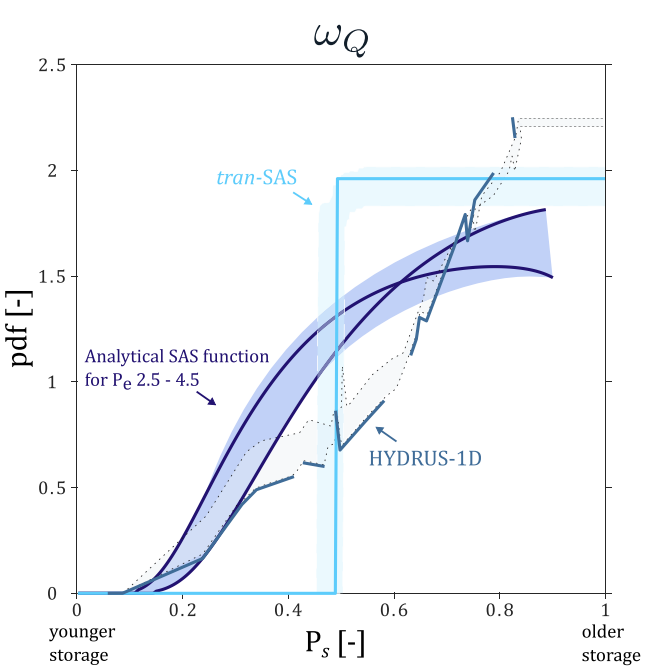

Figure 10. StorAge Selection (SAS) function at the bottom drainage (ω_Q) obtained from the two models (best parameter in solid line and 10–90‰ shown as an uncertainty band) versus the analytical SAS function for estimated Péclet number in the range 2.5–4.5 (shown by the highlight). The solid lines for analytical SAS function illustrate the SAS function for Péclet of 2.5 and 4.5. Analytical SAS function is uncertain at its right tail and, therefore, not depicted here.

sets were used in the simulations as boundary condition. Figure 9 highlights that sole reliance on drainage flow and tracer data (in SAS-based model) may lead to incorrect estimates on the age of evapotranspiration fluxes which is not mitigated by treating evaporation and transpiration as separate fluxes. While physically based models show more robustness in the absence of xylem data, it is the inclusion of xylem tracer data in the calibration process that brings both classes of model into agreement.

4.2. Controls on the Shape of SAS Functions

4.2.1. Bottom Drainage

In the presence of vegetation that transpires a large quantity of water, one wonders how robust are SAS-based approaches. Figure 10 shows that both SAS functions estimated from HYDRUS-1D and *tran*-SAS are well predicted by analytical SAS function derived from a 1-D stationary advection-dispersion equation in which plant water uptake is unaccounted for (Benettin et al., 2013). However, the presence of vegetation indirectly affects the strength of advective forces and the degree of mixing in the system. The average pore velocity estimated from HYDRUS-1D and *tran*-SAS models are in the range 4.4–5.4 [cm d^{-1}] and the longitudinal dispersivity is in the range of 45–100 [cm]. This yields a Péclet number estimate in the range 4.5–2.5. The analytic SAS functions at low Péclet number are highly uncertain and for this reason, are not reported here.

4.2.2. Transpiration

While the shape of SAS functions for the bottom drainage can be reasonably well explained by the interplay between advective and dispersive processes,

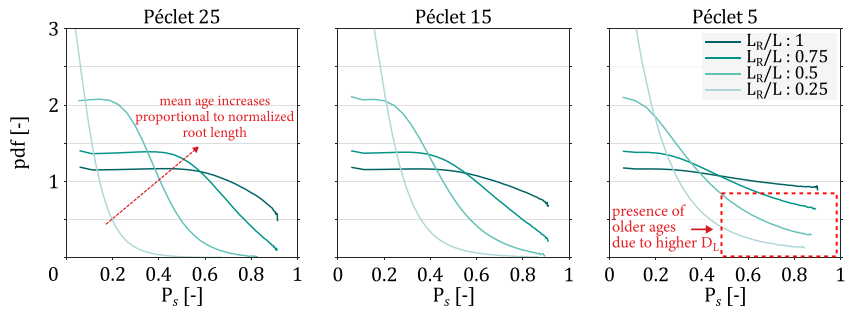

Figure 11. The impact of root length (with uniform shape) on transpiration StorAge Selection (SAS) function. Soil column is $L = 200$ cm, and root length (L_R) is changed to create different ratios of root over column length. Normalized ranked storage is shown on the *x* axis, and the distribution of different ages in storage contributing to the transpiration flux, that is, SAS function of transpiration, is shown on the *y* axis. SAS functions are derived from HYDRUS-1D under different flow regimes represented by diverse Péclet numbers. Varied Péclet numbers are created by changing the strength of dispersion effects, to be specific longitudinal dispersivity. The tail of SAS function is noisy due to numerical truncation (not shown).

studies have not yet explored the role of physical controls on the sampling function for plant transpiration. In the HYDRUS-1D framework, we carried out a virtual experiment which is used to assess the controls on the transpiration SAS function. Initial tests showed that the main parameters affecting the shape of SAS function were the interaction between advective and dispersive processes, and root distribution. Therefore, Péclet numbers of 5, 15, and 25 were chosen to represent a porous medium with high, medium, and low relative strength of dispersion. The impact of root distribution on the shape of SAS functions was studied under these flow regimes. These regimes were created by changing the longitudinal dispersivity (D_L). We estimated SAS functions for transpiration under steady state flow condition to avoid irregular and time-variant shapes. On this basis, 54% of constant daily precipitation P ends up in transpiration ($0.54 \cdot P$) and 6% of it in evaporation ($0.06 \cdot P$). These partitioning of hydrological fluxes are similar to observations during the experiment (see Table 1). Other parameters in this modeling experiment were set to optimal parameters found in the calibration process.

In the first set of simulations, the length of (uniform) roots (i.e., same root density along the entire root zone) is changed under different flow regimes (Figure 11). The mean root-uptake age is directly proportional to the dimensionless root length defined as the length of root zone divided by the total length of the storage volume for all Péclet numbers. Vegetation water uptake is mainly limited to 20–25% youngest water available in the storage when the root length is smaller than one fourth of the length representing the storage domain. As roots grow deeper, the access and uptake of older water increases. When the rooting system enables equal access to all ages available in the storage ($L = L_R$), water uptake affinity becomes similar to random sampling. As one expects, the mean age of water uptake is affected by the interplay of advective and dispersive forces. In highly advective flow regimes (e.g., Pe = 25), a shorter root length implies that only the younger water stored on top of the soil column is accessible, while older water is almost not used. At highly dispersive flow regimes (e.g., Pe = 5), a larger degree of mixing occurs via mechanical dispersion in the system. Therefore, the contribution of older storage does not reach zero because older water is available throughout the column.

The root length is not a good summary metric if the root profile is not uniform, that is, the root density changes along the root zone. Indeed, if the root density is linearly or exponentially decreasing with depth, more water is obviously uptaken from the top than from the lower horizons, if available. As a consequence, comparisons across different profiles are not possible. For this reason, we define a uniform-equivalent root length, that is, $\bar{L}_R$, equal to twice the mean root length μ_{L_R} that is, $\bar{L}_R = 2 \cdot \mu_{L_R}$. The mean root length is estimated by a weighted average across the root zone starting from the surface ($z = 0$) to the deepest point where roots are found ($z = L_R$) using the normalized root length density function $b(z)$. The mean root length is defined here as $\mu_{L_R} = \int_0^{L_R} z \cdot b(z)\, d\tau$ where $\int_0^{L_R} b(z) dz = 1$. By employing these formulations for the linearly decaying root shape with the length of L_R, a mean root length of $1/3L_R$ and a uniform-equivalent root length of $2/3L_R$ are yielded. This means a linearly decreasing root distribution with the length of L_R is comparable with the uniform root shape that is $2/3L_R$ long. Figure 12 illustrates how comparable the SAS function are when different root shapes (uniform versus linearly decaying) share the same uniform-equivalent length in the case L_R is equal to L.

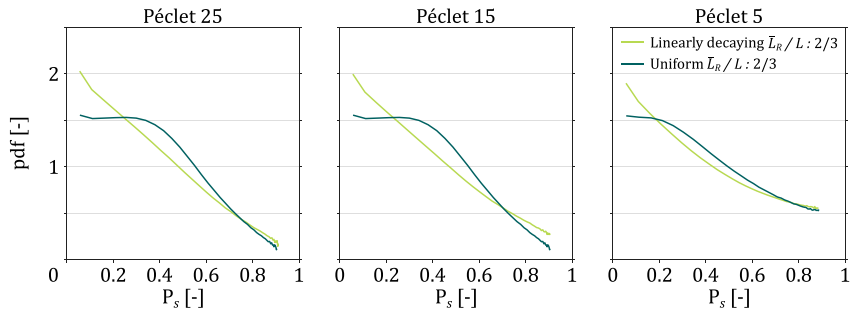

Figure 12. Comparison of transpiration StorAge Selection (SAS) function for different root shapes (uniform versus linearly decaying) with the same uniform-equivalent root length under varied flow regimes. Normalized ranked storage on the *x* axis ranks the water in the storage based on age, and *y* axis shows how transpiration is sampling from the different ages of water in the storage. In this example, the soil column is 2-m long ($L = 200$ cm). The two SAS functions of uniform root length of 133 cm and linearly decaying root length of 200 cm share the same uniform-equivalent root length $(\bar{L}_R)$ and closely approximate one another under all flow regimes, in particular when Péclet number is low. The tail of SAS function is noisy due to numerical truncation (not shown).

The two SAS functions are very similar in the presence of stronger dispersive forces (Pe = 5). At flow regimes with Pe equal to 25 and 15 where advective forces prevail in the system, increased separation is visible between the two SAS functions. However, SAS functions of different root shapes are comparable when they have the same uniform-equivalent length, as one gathers from Figure 11, see also Supporting Information S6 (Section 6 and Figure S7) for further details.

In this context, the ratio of the uniform-equivalent root length $(\bar{L}_R)$ to the length representing the hydrological control volume (L) characterizes with sufficient approximation the age affinity of plant uptake (i.e., the shape of the SAS function for transpiration). In domains with known boundaries, like lysimeters, application of these findings is rather straightforward. At larger scales, approximating a uniform-equivalent root length with the aim of representing entire vegetation stands via field observations seems out of reach with current technologies (but see Section 4.3).

Finally, in our soil-plant-atmosphere system we observed no evidence of stomatal regulation during periods of water stress, and we found no need to consider a dual soil medium in order to capture water uptake patterns. Even though our findings are in line with previous results that emphasize the importance of characterizing the maximum rooting depth to control evapotranspiration (e.g., Camporese et al., 2015; Knighton et al., 2020) at catchment scale, we argue that the methodology proposed here may be also applied to contexts endowed with higher complexity levels. Examples of such cases occur when: a higher degree of stomatal regulation is observed; old water is massively present in immobile soil water, and the bound water composition is markedly different from the mobile soil water (e.g., very dry conditions, or high clay content in soils). Moreover, one may wish to apply this experiment to a larger sample size or a series of replicas for reaffirmation.

4.3. Outlook

One obviously wonders how the current thinking on experimentally closing the mass balance, as exposed above, may be extended to catchment control volumes where large and diverse vegetation assemblages concert spatially heterogeneous transpiration fluxes. Direct measurement of large-scale abstractions entailing massive simultaneous sampling of a representative sample of individual plants (or paradoxically the entire plant community) is definitely out of reach with current technologies because of various constraints. Further research may then focus on the minimum statistically significant sampling effort. However, quite likely the statistical significance of the number of individual plants sampled depends on the specific context, and thus one may hardly hope in some standardized approach.

However, one possibility worth exploring might perhaps rely on proxies and remote sensing. Further research may, in fact, extend toward embedding the parametrization required by computational tools in existing allometric scaling theory, usually termed plant allometry (e.g., Niklas, 1994). Allometry, in this context, would imply inferring reliably belowground biomass, and possibly root length and density as declined above, on the basis of

remote measurables like crown size, tree height, and plant functional group. Several features relevant to transpiration, like the widening of the xylem conduits with plant height, may help to that end (e.g., Katul et al., 2003; Kocillary et al., 2021; Olson et al., 2018). It is also worth noting plant demography plays some role in determining belowground rooting profiles. Plant species will sometimes adapt belowground niches, or the depth of maximally source water when cohabiting with other species (Cabal et al., 2020; Grossiord, Gessler, Granier, Berger, et al., 2014; Parise et al., 2021). At the catchment scale, it would be important to consider such demography.

Though direct measurement of actual transpiration at large-scale is still a major challenge, remotely acquired and objectively manipulated information on above-ground data (e.g., Camps-Valls et al., 2013; Tuia et al., 2011) may generate spatially explicit maps of transpiration fluxes by suitable earth monitoring with statistical learning where traditional sampling may serve as ground truthing. Large assemblages of vegetation may thus be linked to parametrizations like the ones pursued herein, relating them to observables like plant aboveground biomass, crown size, height, and taxonomy. However, current allometric models include untested (or at least leniently challenged) assumptions and often a large number of parameters, making it difficult to frame properly the reliability of the predictions they make relative to the controls identified in this paper.

There are various elements that make it difficult to define the water balance at the catchment scale, including for example, the quantification of nonprecipitation water inputs and canopy interception. In terms of transport processes, exploring whether remote sensing and plant allometry may provide the missing link toward a closure of the mass balance for whole catchment scales is the main goal of forthcoming work in this domain.

5. Conclusions

The main conclusions of this paper are summarized as follows:

1. While sole reliance on drainage and tracer data was shown to be misleading in inferring the age dynamics of transpiration, integrating such data with soil water isotopic composition and accurate approximation on plant root distribution might lead to close predictions on temporal origins of vegetation water use in physically based models
2. Synergistic use of drainage, soil and plant tracer data, improves understanding on age of plant water uptake and leads to convergence of predictions from different classes of models
3. Such convergence and links allow parametrization of the age of water uptake in transport models which might be helpful when transferring it to large scales; and therefore, are vital
4. The most significant influence on the age of water in drainage is the interplay between the advective and dispersive forces even when a substantial amount of water entering the storage is taken up by vegetation
5. The presence of vegetation seems to have impacts on the degree of mixing in the storage and the soil hydraulic parameters; therefore, it indirectly affects the drainage age distribution
6. In this study we showed that root distribution bears the largest influence on the age distribution of transpiration. The effect of which was lumped into the introduced parameter *uniform-equivalent root length*
7. The ratio of the uniform-equivalent root length to the representative length of the hydrological domain was shown to primarily drive the age of water extracted by plants
8. The plants' age statistics are comparable for distinct root shapes across their uniform-equivalent root length

Acknowledgments
AR and PB thank ENAC school at EPFL for financial support and acknowledge the Swiss National Science Foundation Grant No. CRSII5_186422. We thank Dyan Pratt for her help in conducting the experiment, Kim Janzen for laser and mass spectrometry isotopic analysis, and ECHO lab members for their help in intensive characterization of the system. We also thank Florian Heinlein, Jannis Groh and one anonymous reviewer for the useful comments provided. Open access funding provided by Ecole Polytechnique Federale de Lausanne.

Data Availability Statement

All data presented in this paper are available at http://doi.org/10.5281/zenodo.4037240 (Nehemy et al., 2020), under Creative Commons Attribution (CC BY) license.

References

Allen, S. T., Kirchner, J. W., Braun, S., Siegwolf, R. T., & Goldsmith, G. R. (2019). Seasonal origins of soil water used by trees. *Hydrology and Earth System Sciences*, *23*(2), 1199–1210. https://doi.org/10.5194/hess-23-1199-2019

Asadollahi, M., Stumpp, C., Rinaldo, A., & Benettin, P. (2020). Transport and water age dynamics in soils: A comparative study of spatially integrated and spatially explicit models. *Water Resources Research*, *56*, e2019WR025539. https://doi.org/10.1029/2019WR025539

Baram, S., Couvreur, V., Harter, T., Read, M., Brown, P., Kandelous, M., et al. (2016). Estimating nitrate leaching to groundwater from orchards: Comparing crop nitrogen excess, deep vadose zone data-driven estimates, and HYDRUS modeling. *Vadose Zone Journal*, *15*(11), 1–13. https://doi.org/10.2136/vzj2016.07.0061

Bear, J. (2012). *Hydraulics of groundwater*. Courier Corporation.

Benettin, P., & Bertuzzo, E. (2018). tran-SAS v1. 0: A numerical model to compute catchment-scale hydrologic transport using storage selection functions. *Geoscientific Model Development*, *11*(4), 1627–1639. https://doi.org/10.5194/gmd-11-1627-2018

Benettin, P., Nehemy, M. F., Asadollahi, M., Pratt, D., Bensimon, M., McDonnell, J. J., & Rinaldo, A. (2021). Tracing and closing the water balance in a vegetated lysimeter. *Water Resources Research*, *57*, e2020WR029049. https://doi.org/10.1029/2020WR029049

Benettin, P., Nehemy, M. F., Cernusak, L. A., Kahmen, A., & McDonnell, J. J. (2021). On the use of leaf water to determine plant water source: A proof of concept. *Hydrological Processes*, *35*, e14073. https://doi.org/10.1002/hyp.14073

Benettin, P., Rinaldo, A., & Botter, G. (2013). Kinematics of age mixing in advection-dispersion models. *Water Resources Research*, *49*, 8539–8551. https://doi.org/10.1002/2013WR014708

Benettin, P., Soulsby, C., Birkel, C., Tetzlaff, D., Botter, G., & Rinaldo, A. (2017). Using SAS functions and high-resolution isotope data to unravel travel time distributions in headwater catchments. *Water Resources Research*, *53*, 1864–1878. https://doi.org/10.1002/2016WR020117

Bertuzzo, E., Thomet, M., Botter, G., & Rinaldo, A. (2013). Catchment-scale herbicides transport: Theory and application. *Advances in Water Resources*, *52*, 232–242. https://doi.org/10.1016/j.advwatres.2012.11.007

Botter, G., Bertuzzo, E., & Rinaldo, A. (2011). Catchment residence and travel time distributions: The master equation. *Geophysical Research Letters*, *38*, L11403. https://doi.org/10.1029/2011GL047666

Bowen, G. J., Putman, A., Brooks, J. R., Bowling, D. R., Oerter, E. J., & Good, S. P. (2018). Inferring the source of evaporated waters using stable h and o isotopes. *Oecologia*, *187*(4), 1025–1039. https://doi.org/10.1007/s00442-018-4192-5

Brinkmann, N., Seeger, S., Weiler, M., Buchmann, N., Eugster, W., & Kahmen, A. (2018). Employing stable isotopes to determine the residence times of soil water and the temporal origin of water taken up by *Fagus sylvatica* and *Picea abies* in a temperate forest. *New Phytologist*, *219*(4), 1300–1313. https://doi.org/10.1111/nph.15255

Brooks, J. R., Barnard, H. R., Coulombe, R., & McDonnell, J. J. (2010). Ecohydrologic separation of water between trees and streams in a Mediterranean climate. *Nature Geoscience*, *3*(2), 100–104. https://doi.org/10.1038/ngeo722

Brunel, J.-P., Walker, G. R., & Kennett-Smith, A. K. (1995). Field validation of isotopic procedures for determining sources of water used by plants in a semi-arid environment. *Journal of Hydrology*, *167*(1–4), 351–368. https://doi.org/10.1016/0022-1694(94)02575-v

Buzacott, A. J., van derVelde, Y., Keitel, C., & Vervoort, R. W. (2020). Constraining water age dynamics in a south-eastern Australian catchment using an age-ranked storage and stable isotope approach. *Hydrological Processes*, *34*(23), 4384–4403. https://doi.org/10.1002/hyp.13880

Cabal, C., Martínez-García, R., de Castro Aguilar, A., Valladares, F., & Pacala, S. W. (2020). The exploitative segregation of plant roots. *Science*, *370*(6521), 1197–1199. https://doi.org/10.1126/science.aba9877

Cai, G., Vanderborght, J., Couvreur, V., Mboh, C. M., & Vereecken, H. (2018). Parameterization of root water uptake models considering dynamic root distributions and water uptake compensation. *Vadose Zone Journal*, *17*(1), 1–21. https://doi.org/10.2136/vzj2016.12.0125

Camporese, M., Daly, E., & Paniconi, C. (2015). Catchment-scale Richards equation-based modeling of evapotranspiration via boundary condition switching and root water uptake schemes. *Water Resources Research*, *51*, 5756–5771. https://doi.org/10.1002/2015WR017139

Camps-Valls, G., Tuia, D., & Benediktsson, J. (2013). Advances in hyperspectral image classification: Earth monitoring with statistical learning methods. *IEEE Signal Processing Magazine*, *31*(1), 45–54.

Cavallaro, A., Carbonell Silleta, L., Pereyra, D. A., Goldstein, G., Scholz, F. G., & Bucci, S. J. (2020). Foliar water uptake in arid ecosystems: Seasonal variability and ecophysiological consequences. *Oecologia*, *193*, 337–348. https://doi.org/10.1007/s00442-020-04673-1

Couvreur, V., Vanderborght, J., Beff, L., & Javaux, M. (2014). Horizontal soil water potential heterogeneity: Simplifying approaches for crop water dynamics models. *Hydrology and Earth System Sciences*, *18*(5), 1723–1743. https://doi.org/10.5194/hess-18-1723-2014

Dawson, T. E., & Goldsmith, G. R. (2018). The value of wet leaves. *New Phytologist*, *219*(4), 1156–1169. https://doi.org/10.1111/nph.15307

Dawson, T. E., Mambelli, S., Plamboeck, A. H., Templer, P. H., & Tu, K. P. (2002). Stable isotopes in plant ecology. *Annual Review of Ecology and Systematics*, *33*(1), 507–559. https://doi.org/10.1146/annurev.ecolsys.33.020602.095451

Dubbert, M., Caldeira, M. C., Dubbert, D., & Werner, C. (2019). A pool-weighted perspective on the two-water-worlds hypothesis. *New Phytologist*, *222*(3), 1271–1283. https://doi.org/10.1111/nph.15670

Dubbert, M., & Werner, C. (2019). Water fluxes mediated by vegetation: Emerging isotopic insights at the soil and atmosphere interfaces. *New Phytologist*, *221*(4), 1754–1763. https://doi.org/10.1111/nph.15547

Ehleringer, J., & Dawson, T. (1992). Water uptake by plants: Perspectives from stable isotope composition. *Plant, Cell and Environment*, *15*(9), 1073–1082. https://doi.org/10.1111/j.1365-3040.1992.tb01657.x

Evaristo, J., Jasechko, S., & McDonnell, J. J. (2015). Global separation of plant transpiration from groundwater and streamflow. *Nature*, *525*(7567), 91–94. https://doi.org/10.1038/nature14983

Evaristo, J., Kim, M., van Haren, J., Pangle, L. A., Harman, C. J., Troch, P. A., & McDonnell, J. J. (2019). Characterizing the fluxes and age distribution of soil water, plant water, and deep percolation in a model tropical ecosystem. *Water Resources Research*, *55*, 3307–3327. https://doi.org/10.1029/2018WR023265

Fatichi, S., Pappas, C., & Ivanov, V. Y. (2016). Modeling plant-water interactions: An ecohydrological overview from the cell to the global scale. *Wiley Interdisciplinary Reviews: Water*, *3*(3), 327–368. https://doi.org/10.1002/wat2.1125

Feddes, R. A. (1982). *Simulation of field water use and crop yield*. Pudoc.

Feddes, R. A., Hoff, H., Bruen, M., Dawson, T., De Rosnay, P., Dirmeyer, P., et al. (2001). Modeling root water uptake in hydrological and climate models. *Bulletin of the American Meteorological Society*, *82*(12), 2797–2810. https://doi.org/10.1175/1520-0477(2001)082<2797:MRWUIH>2.3.CO;2

Feldman, A. F., Short Gianotti, D. J., Konings, A. G., Gentine, P., & Entekhabi, D. (2021). Patterns of plant rehydration and growth following pulses of soil moisture availability. *Biogeosciences*, *18*(3), 831–847. https://doi.org/10.5194/bg-18-831-2021

Geris, J., Tetzlaff, D., McDonnell, J. J., & Soulsby, C. (2017). Spatial and temporal patterns of soil water storage and vegetation water use in humid northern catchments. *Science of the Total Environment*, *595*, 486–493. https://doi.org/10.1016/j.scitotenv.2017.03.275

Goldsmith, G. R., Lehmann, M. M., Cernusak, L. A., Arend, M., & Siegwolf, R. T. (2017). Inferring foliar water uptake using stable isotopes of water. *Oecologia*, *184*(4), 763–766. https://doi.org/10.1007/s00442-017-3917-1

Goldsmith, G. R., Muñoz-Villers, L. E., Holwerda, F., McDonnell, J. J., Asbjornsen, H., & Dawson, T. E. (2012). Stable isotopes reveal linkages among ecohydrological processes in a seasonally dry tropical montane cloud forest. *Ecohydrology*, *5*(6), 779–790. https://doi.org/10.1002/eco.268

Groh, J., Stumpp, C., Lücke, A., Pütz, T., Vanderborght, J., & Vereecken, H. (2018). Inverse estimation of soil hydraulic and transport parameters of layered soils from water stable isotope and lysimeter data. *Vadose Zone Journal*, *17*(1), 1–19. https://doi.org/10.2136/vzj2017.09.0168

Grossiord, C., Gessler, A., Granier, A., Berger, S., Bréchet, C., Hentschel, R., & Bonal, D. (2014). Impact of interspecific interactions on the soil water uptake depth in a young temperate mixed species plantation. *Journal of Hydrology*, *519*, 3511–3519. https://doi.org/10.1016/j.jhydrol.2014.11.011

Grossiord, C., Gessler, A., Granier, A., Pollastrini, M., Bussotti, F., & Bonal, D. (2014). Interspecific competition influences the response of oak transpiration to increasing drought stress in a mixed Mediterranean forest. *Forest Ecology and Management*, *318*, 54–61. https://doi.org/10.1016/j.foreco.2014.01.004

Haghighi, E., & Kirchner, J. W. (2017). Near-surface turbulence as a missing link in modeling evapotranspiration-soil moisture relationships. *Water Resources Research*, *53*, 5320–5344. https://doi.org/10.1002/2016WR020111

Harman, C. J. (2015). Time-variable transit time distributions and transport: Theory and application to storage-dependent transport of chloride in a watershed. *Water Resources Research*, *51*, 1–30. https://doi.org/10.1002/2014WR015707

Harman, C. J., Rao, P., Basu, N., McGrath, G., Kumar, P., & Sivapalan, M. (2011). Climate, soil, and vegetation controls on the temporal variability of vadose zone transport. *Water Resources Research*, *47*, WO0J13. https://doi.org/10.1029/2010WR010194

Jarvis, N. (1989). A simple empirical model of root water uptake. *Journal of Hydrology*, *107*(1–4), 57–72. https://doi.org/10.1016/0022-1694(89)90050-4

Johnson, M. S., & Jost, G. (2011). Ecohydrology and biogeochemistry of the rhizosphere in forested ecosystems. In *Forest hydrology and biogeochemistry* (pp. 483–498). Springer. https://doi.org/10.1007/978-94-007-1363-5_24

Katul, G., Leuning, R., & Oren, R. (2003). Relationship between plant hydraulic and biochemical properties derived from a steady-state coupled water and carbon transport model. *Plant, Cell and Environment*, *26*, 339–350. https://doi.org/10.1046/j.1365-3040.2003.00965.x

Kendall, C., & McDonnell, J. J. (1998). *Isotope tracers in catchment hydrology*. Elsevier.

Knighton, J., Singh, K., & Evaristo, J. (2020). Understanding catchment-scale forest root water uptake strategies across the continental United States through inverse ecohydrological modeling. *Geophysical Research Letters*, *47*, e2019GL085937. https://doi.org/10.1029/2019GL085937

Kocillary, L., Olson, M., Suweis, S., Rocha, R., Lovison, A., Cardin, F., & Maritan, A. (2021). The widened pipe model of plant hydraulic evolution. *Proceedings of the US National Academy of Sciences of the United States of America*, *118*(22), e2100314118.

Kuppel, S., Tetzlaff, D., Maneta, M. P., & Soulsby, C. (2018). EcH2O-iso 1.0: Water isotopes and age tracking in a process-based, distributed ecohydrological model. *Geoscientific Model Development*, *11*(7), 3045–3069. https://doi.org/10.5194/gmd-11-3045-2018

Lehmann, P., Assouline, S., & Or, D. (2008). Characteristic lengths affecting evaporative drying of porous media. *Physical Review E*, *77*(5), 056309. https://doi.org/10.1103/physreve.77.056309

Lehmann, P., Bickel, S., Wei, Z., & Or, D. (2020). Physical constraints for improved soil hydraulic parameter estimation by pedotransfer functions. *Water Resources Research*, *56*, e2019WR025963. https://doi.org/10.1029/2019WR025963

Li, L., Sullivan, P. L., Benettin, P., Cirpka, O. A., Bishop, K., Brantley, S. L., et al. (2021). Toward catchment hydro-biogeochemical theories. *Wiley Interdisciplinary Reviews: Water*, *8*(1), e1495. https://doi.org/10.1002/wat2.1495

Limm, E. B., & Dawson, T. E. (2010). *Polystichum munitum* (dryopteridaceae) varies geographically in its capacity to absorb fog water by foliar uptake within the redwood forest ecosystem. *American Journal of Botany*, *97*(7), 1121–1128. https://doi.org/10.3732/ajb.1000081

Lindroth, A., & Cienciala, E. (1996). Water use efficiency of short-rotation salix viminalis at leaf, tree and stand scales. *Tree Physiology*, *16*(1–2), 257–262. https://doi.org/10.1093/treephys/16.1-2.257

Maxwell, R. M., Condon, L. E., Danesh-Yazdi, M., & Bearup, L. A. (2019). Exploring source water mixing and transient residence time distributions of outflow and evapotranspiration with an integrated hydrologic model and Lagrangian particle tracking approach. *Ecohydrology*, *12*(1), e2042. https://doi.org/10.1002/eco.2042

McCutcheon, R. J., McNamara, J. P., Kohn, M. J., & Evans, S. L. (2017). An evaluation of the ecohydrological separation hypothesis in a semiarid catchment. *Hydrological Processes*, *31*(4), 783–799. https://doi.org/10.1002/hyp.11052

McDonnell, J. J. (2014). The two water worlds hypothesis: Ecohydrological separation of water between streams and trees? *Wiley Interdisciplinary Reviews: Water*, *1*(4), 323–329. https://doi.org/10.1002/wat2.1027

Mook, W., & Rozanski, K. (2000). Environmental isotopes in the hydrological cycle. In *Principles and applications, Volumes I, IV and V*. International Atomic Energy Agency and United Nations Educational, Scientific and Cultural Organization.

Mualem, Y. (1976). A new model for predicting the hydraulic conductivity of unsaturated porous media. *Water Resources Research*, *12*(3), 513–522. https://doi.org/10.1029/WR012i003p00513

Nehemy, M. F., Benettin, P., Asadollahi, M., Pratt, D., Rinaldo, A., & McDonnell, J. J. (2020). Dataset: The SPIKE II experiment—Tracing the water balance. *Zenodo*. https://doi.org/10.5281/zenodo.4037240

Nehemy, M. F., Benettin, P., Asadollahi, M., Pratt, D., Rinaldo, A., & McDonnell, J. J. (2021). Tree water deficit and dynamic source water partitioning. *Hydrological Processes*, *35*(1), e14004. https://doi.org/10.1002/hyp.14004

Niklas, K. J. (1994). *Plant allometry: The scaling of form and process*. University of Chicago Press.

Olson, M. E., Soriano, D., Rosell, J. A., Anfodillo, T., Donoghue, M. J., Edwards, E. J., et al. (2018). Plant height and hydraulic vulnerability to drought and cold. *Proceedings of the National Academy of Sciences of the United States of America*, *115*(29), 7551–7556. https://doi.org/10.1073/pnas.1721728115

Or, D., Lehmann, P., Shahraeeni, E., & Shokri, N. (2013). Advances in soil evaporation physics—A review. *Vadose Zone Journal*, *12*(4), 1–16. https://doi.org/10.2136/vzj2012.0163

Parise, A. G., Bertoli, S. C., & Souza, G. M. (2021). Belowground interactions affect shoot growth in *Eucalyptus urophylla* under restrictive conditions. *Plant Signaling & Behavior*, *16*(9), 1927589. https://doi.org/10.1080/15592324.2021.1927589

Penna, D., Hopp, L., Scandellari, F., Allen, S. T., Benettin, P., Beyer, M., et al. (2018). Ideas and perspectives: Tracing terrestrial ecosystem water fluxes using hydrogen and oxygen stable isotopes—Challenges and opportunities from an interdisciplinary perspective. *Biogeosciences*, *15*(21), 6399–6415. https://doi.org/10.5194/bg-15-6399-2018

Porporato, A., Daly, E., & Rodriguez-Iturbe, I. (2004). Soil water balance and ecosystem response to climate change. *The American Naturalist*, *164*(5), 625–632. https://doi.org/10.1086/424970

Pütz, T., Kiese, R., Wollschläger, U., Groh, J., Rupp, H., Zacharias, S., et al. (2016). TERENO-SOILCan: A lysimeter-network in Germany observing soil processes and plant diversity influenced by climate change. *Environmental Earth Sciences*, *75*(18), 1–14. https://doi.org/10.1007/s12665-016-6031-5

Quade, M., Klosterhalfen, A., Graf, A., Brüggemann, N., Hermes, N., Vereecken, H., & Rothfuss, Y. (2019). In-situ monitoring of soil water isotopic composition for partitioning of evapotranspiration during one growing season of sugar beet (*Beta vulgaris*). *Agricultural and Forest Meteorology*, *266*, 53–64. https://doi.org/10.1016/j.agrformet.2018.12.002

Queloz, P., Carraro, L., Benettin, P., Botter, G., Rinaldo, A., & Bertuzzo, E. (2015). Transport of fluorobenzoate tracers in a vegetated hydrologic control volume: 2. Theoretical inferences and modeling. *Water Resources Research*, *51*, 2793–2806. https://doi.org/10.1002/2014WR016508

Remondi, F., Kirchner, J. W., Burlando, P., & Fatichi, S. (2018). Water flux tracking with a distributed hydrological model to quantify controls on the spatio-temporal variability of transit time distributions. *Water Resources Research*, *54*, 3081–3099. https://doi.org/10.1002/2017WR021689

Richards, L. (1931). Soil-water conduction of liquids in porous mediums. *Physics*, *1*, 318–333. https://doi.org/10.1063/1.1745010

Rinaldo, A., Benettin, P., Harman, C. J., Hrachowitz, M., McGuire, K. J., Van Der Velde, Y., & Botter, G. (2015). Storage selection functions: A coherent framework for quantifying how catchments store and release water and solutes. *Water Resources Research*, *51*, 4840–4847. https://doi.org/10.1002/2015WR017273

Schneider, J., Groh, J., Pütz, T., Helmig, R., Rothfuss, Y., Vereecken, H., & Vanderborght, J. (2021). Prediction of soil evaporation measured with weighable lysimeters using the FAO Penman-Monteith method in combination with Richards' equation. *Vadose Zone Journal*, *20*(1), e20102. https://doi.org/10.1002/vzj2.20102

Seeger, S., & Weiler, M. (2021). Temporal dynamics of tree xylem water isotopes: In-situ monitoring and modelling. *Biogeosciences Discussions*, *18*, 4063–4627.

Šimůnek, J., & Hopmans, J. W. (2009). Modeling compensated root water and nutrient uptake. *Ecological Modelling*, *220*(4), 505–521.

Simunek, J., Sejna, M., & Van Genuchten, M. T. (1999). *The HYDRUS-2d software package*. International Ground Water Modeling Center.

Simunek, J., Sejna, M., Van Genuchten, M. T., Simunek, J., Sejna, M., Jacques, D., & Sakai, M. (1998). *HYDRUS-1D. Simulating the one-dimensional movement of water, heat, and multiple solutes in variably-saturated media, version, 2*. CSIRO.

Sprenger, M., & Allen, S. T. (2020). What ecohydrologic separation is and where we can go with it. *Water Resources Research*, *56*, e2020WR027238. https://doi.org/10.1029/2020WR027238

Sprenger, M., Seeger, S., Blume, T., & Weiler, M. (2016). Travel times in the vadose zone: Variability in space and time. *Water Resources Research*, *52*, 5727–5754. https://doi.org/10.1002/2015wr018077

Sprenger, M., Stumpp, C., Weiler, M., Aeschbach, W., Allen, S. T., Benettin, P., et al. (2019). The demographics of water: A review of water ages in the critical zone. *Reviews of Geophysics*, *57*, 800–834. https://doi.org/10.1029/2018RG000633

Sprenger, M., Tetzlaff, D., Buttle, J., Laudon, H., Leistert, H., Mitchell, C. P., & Soulsby, C. (2018). Measuring and modeling stable isotopes of mobile and bulk soil water. *Vadose Zone Journal*, *17*(1), 1–18. https://doi.org/10.2136/vzj2017.08.0149

Sprenger, M., Tetzlaff, D., Buttle, J., Laudon, H., & Soulsby, C. (2018). Water ages in the critical zone of long-term experimental sites in northern latitudes. *Hydrology and Earth System Sciences*, *22*(7), 3965–3981. https://doi.org/10.5194/hess-22-3965-2018

Sprenger, M., Volkmann, T. H., Blume, T., & Weiler, M. (2015). Estimating flow and transport parameters in the unsaturated zone with pore water stable isotopes. *Hydrology and Earth System Sciences*, *19*(6), 2617–2635. https://doi.org/10.5194/hess-19-2617-2015

Stumpp, C., Maloszewski, P., Stichler, W., & Fank, J. (2009). Environmental isotope (δ^{18}O) and hydrological data to assess water flow in unsaturated soils planted with different crops: Case study lysimeter station "wagna" (AuAustria). *Journal of Hydrology*, *369*(1–2), 198–208. https://doi.org/10.1016/j.jhydrol.2009.02.047

Stumpp, C., Stichler, W., Kandolf, M., & Šimůnek, J. (2012). Effects of land cover and fertilization method on water flow and solute transport in five lysimeters: A long-term study using stable water isotopes. *Vadose Zone Journal*, *11*(1), vzj2011.0075. https://doi.org/10.2136/vzj2011.0075

Sudicky, E. A. (1986). A natural gradient experiment on solute transport in a sand aquifer: Spatial variability of hydraulic conductivity and its role in the dispersion process. *Water Resources Research*, *22*(13), 2069–2082. https://doi.org/10.1029/WR022i013p02069

Tuia, D., Volpi, M., Copa, L., Kanevski, M., & Munoz-Mari, J. (2011). A survey of active learning algorithms for supervised remote sensing image classification. *IEEE Journal of Selected Topics in Signal Processing*, *5*(3), 606–617. https://doi.org/10.1109/jstsp.2011.2139193

Van der Velde, Y., De Rooij, G., Rozemeijer, J., Van Geer, F., & Broers, H. (2010). Nitrate response of a lowland catchment: On the relation between stream concentration and travel time distribution dynamics. *Water Resources Research*, *46*, W11534. https://doi.org/10.1029/2010WR009105

Van Der Velde, Y., Torfs, P., Van Der Zee, S., & Uijlenhoet, R. (2012). Quantifying catchment-scale mixing and its effect on time-varying travel time distributions. *Water Resources Research*, *48*, W06536. https://doi.org/10.1029/2011WR011310

Van Genuchten, M. T. (1980). A closed-form equation for predicting the hydraulic conductivity of unsaturated soils. *Soil Science Society of America Journal*, *44*(5), 892–898. https://doi.org/10.2136/sssaj1980.03615995004400050002x

Volkmann, T. H., Haberer, K., Gessler, A., & Weiler, M. (2016). High-resolution isotope measurements resolve rapid ecohydrological dynamics at the soil-plant interface. *New Phytologist*, *210*(3), 839–849. https://doi.org/10.1111/nph.13868

von Freyberg, J., Allen, S. T., Grossiord, C., & Dawson, T. E. (2020). Plant and root-zone water isotopes are difficult to measure, explain, and predict: Some practical recommendations for determining plant water sources. *Methods in Ecology and Evolution*, *11*(11), 1352–1367. https://doi.org/10.1111/2041-210x.13461

Vrugt, J. A. (2016). Markov chain Monte Carlo simulation using the dream software package: Theory, concepts, and Matlab implementation. *Environmental Modelling & Software*, *75*, 273–316. https://doi.org/10.1016/j.envsoft.2015.08.013

Wenninger, J., Beza, D. T., & Uhlenbrook, S. (2010). Experimental investigations of water fluxes within the soil–vegetation–atmosphere system: Stable isotope mass-balance approach to partition evaporation and transpiration. *Physics and Chemistry of the Earth, Parts A/B/C*, *35*(13–14), 565–570. https://doi.org/10.1016/j.pce.2010.07.016

Zhang, S., Wen, X., Wang, J., Yu, G., & Sun, X. (2010). The use of stable isotopes to partition evapotranspiration fluxes into evaporation and transpiration. *Acta Ecologica Sinica*, *30*(4), 201–209. https://doi.org/10.1016/j.chnaes.2010.06.003

Zimmermann, U., Ehhalt, D., & Münnich, K. (1967). Soil-water movement and evapotranspiration: Changes in the isotopic composition of the water. In *Isotopes in hydrology. Proceedings of a symposium*(pp. 567–584). IAEA.